



Observing wind, aerosol particles, cloud and precipitation: Finland's new ground-based remote-sensing network

A. Hirsikko^{1,2}, E. J. O'Connor^{1,3}, M. Komppula⁴, K. Korhonen⁴, A. Pfüller⁴, E. Giannakaki⁴, C. R. Wood¹, M. Bauer-Pfundstein⁵, A. Poikonen¹, T. Karppinen⁶, H. Lonka¹, M. Kurri¹, J. Heinonen¹, D. Moisseev⁷, E. Asmi¹, V. Aaltonen¹, A. Nordbo⁷, E. Rodriguez¹, H. Lihavainen¹, A. Laaksonen¹, K. E. J. Lehtinen^{4,8}, T. Laurila¹, T. Petäjä⁹, M. Kulmala⁹, and Y. Viisanen¹

¹Finnish Meteorological Institute, P.O. Box 503, 00101 Helsinki, Finland

²Forschungszentrum Jülich GmbH, Institut für Energie- und Klimaforschung: Troposphäre (IEK-8), Jülich, Germany

³Meteorology Department, University of Reading, Reading, UK

⁴Finnish Meteorological Institute, P.O. Box 1627, 70211 Kuopio, Finland

⁵Meteorologische Messtechnik GmbH (METEK), Elmshorn, Germany

⁶Finnish Meteorological Institute, Tähteläntie 62, 99600 Sodankylä, Finland

⁷Dept. of Physics, University of Helsinki, P.O. Box 48, 00014 Helsinki, Finland

⁸University of Eastern Finland, Dept. Applied Physics, P.O. Box 1627, 70211 Kuopio, Finland

⁹Dept. of Physics, University of Helsinki, P.O. Box 64, 00014 Helsinki, Finland

Correspondence to: A. Hirsikko (anne.hirsikko@fmi.fi; a.hirsikko@fz-juelich.de)

Received: 27 June 2013 – Published in Atmos. Meas. Tech. Discuss.: 8 August 2013

Revised: 17 March 2014 – Accepted: 19 March 2014 – Published: 19 May 2014

Abstract. The Finnish Meteorological Institute, in collaboration with the University of Helsinki, has established a new ground-based remote-sensing network in Finland. The network consists of five topographically, ecologically and climatically different sites distributed from southern to northern Finland. The main goal of the network is to monitor air pollution and boundary layer properties in near real time, with a Doppler lidar and ceilometer at each site. In addition to these operational tasks, two sites are members of the Aerosols, Clouds and Trace gases Research InfraStructure Network (ACTRIS); a K_a band cloud radar at Sodankylä will provide cloud retrievals within CloudNet, and a multi-wavelength Raman lidar, Polly^{XT} (PORTable Lidar sYSTEM eXTended), in Kuopio provides optical and microphysical aerosol properties through EARLINET (the European Aerosol Research Lidar Network). Three C-band weather radars are located in the Helsinki metropolitan area and are deployed for operational and research applications. We performed two inter-comparison campaigns to investigate the Doppler lidar

performance, compare the backscatter signal and wind profiles, and to optimize the lidar sensitivity through adjusting the telescope focus length and data-integration time to ensure sufficient signal-to-noise ratio (SNR) in low-aerosol-content environments. In terms of statistical characterization, the wind-profile comparison showed good agreement between different lidars. Initially, there was a discrepancy in the SNR and attenuated backscatter coefficient profiles which arose from an incorrectly reported telescope focus setting from one instrument, together with the need to calibrate. After diagnosing the true telescope focus length, calculating a new attenuated backscatter coefficient profile with the new telescope function and taking into account calibration, the resulting attenuated backscatter profiles all showed good agreement with each other. It was thought that harsh Finnish winters could pose problems, but, due to the built-in heating systems, low ambient temperatures had no, or only a minor, impact on the lidar operation – including scanning-head motion. However, accumulation of snow and ice on the lens

has been observed, which can lead to the formation of a water/ice layer thus attenuating the signal inconsistently. Thus, care must be taken to ensure continuous snow removal.

1 Introduction

Polar areas have been observed to be especially vulnerable to climate change (ACIA, 2005; IPCC, 2007). Several factors influence global climate change. Clouds are a major component in the global hydrological cycle – for example by storing, transporting and redistributing water. Clouds also contribute to global energy balance through reflecting, transmitting and radiating solar energy. Cloud properties (e.g. albedo, precipitation rate and lifetime) depend, amongst other factors, on the number concentration of aerosol particles and on their chemical composition (Twomey, 1974; Albrecht, 1989; Lohmann and Feichter, 2005). Despite intensive research, the interaction between aerosol particles and clouds is still one of the least-understood elements of Earth's climate (McFiggans et al., 2006), with uncertainty arising from: (i) environment-dependent sources of primary and secondary particles, (ii) varying spatial and temporal distribution and composition of aerosol particles, (iii) cloud and below-cloud dynamics, microphysics and precipitation (e.g. Chen and Penner, 2005; Hegg et al., 2012; Makkonen et al., 2012). In addition to indirect climate effects, aerosol particles have hazardous health effects and direct atmospheric radiative impacts (Haywood and Boucher, 2000; IPCC, 2007; Myhre, 2009). There is a sensitive balance between certain factors cooling, and other factors warming, the climate. Assessment of these factors contributing to climate change requires careful research at the process level, in order to implement suitable parameterizations in global-scale models (IPCC, 2007; Lohmann et al., 2010).

Clouds, and their interaction with the environment, have been investigated through in situ airborne measurements (e.g. Heymsfield et al., 2002), ground-based campaigns (e.g. Verheggen et al., 2007; Lihavainen et al., 2010; Kamphus et al., 2010) or continuous observations (e.g. Marinoni et al., 2004; Portin et al., 2009). In situ observations provide information at the process level; however, airborne measurements are expensive, and thus the number of observations is limited. In situ ground-based observations require cloud-base to be low enough for the station to be inside the cloud. Both of these methods lack the columnar information on cloud layers, their dynamics and optical properties. Satellite and ground-based remote-sensing techniques have been developed for cloud-profile investigations. Synergy of light/radio detecting and ranging (i.e. lidar, ceilometer and radar) techniques has provided breakthroughs for cloud dynamical and microphysical research at fine temporal and spatial resolution (e.g. O'Connor et al., 2005; Westbrook et al., 2010a, b). Ideally, a combination of

in situ and remote-sensing observations would provide the best basis for process-level research of clouds. Assessment of cloud-profile climatologies from satellite (Delanoë et al., 2011) and ground-based active instrumentation (Illingworth et al., 2007) is useful for global climate and weather forecast modelling. However, despite the development of instrumentation and data-analysis techniques, an understanding of the full coupling between cloud processes and their subsequent feedback mechanisms is still required (Bony et al., 2006).

With regard to aerosol particles, their emission rates, the quantity and quality of sources, distribution within the atmospheric boundary layer (ABL), and subsequent entrainment into the free troposphere – all have an effect on atmospheric radiative properties and air quality. Forest fires emit aerosol particles with strong climate and health impacts, and volcanic eruptions are hazardous for aviation with an immediate impact on the economy, and hence, for such events, real-time knowledge of the transport, dispersion and extent of the ash plume in the atmosphere is crucial. During the Iceland volcanic eruptions in 2010, research institutes in some European countries were well prepared to monitor ash plumes in the troposphere (e.g. Ansmann et al., 2011; Sicard et al., 2012; Revuelta et al., 2010; Rolf et al., 2012; Pappalardo et al., 2013). Ash layers were detected, and particularly well identified with lidars with depolarization capability. In Finland, only a short observation period with a Raman lidar was possible in Helsinki, from which it was possible to identify the ash plume from the Grimsvötn volcano as it passed over Finland in the spring of 2011. Despite the lack of comprehensive remote-sensing observations, balloon-borne in situ measurements were performed in order to characterize the volcanic ash particulate properties (Petäjä et al., 2012). Experimental investigation of aerosol particle climatology requires columnar information of aerosol particle properties, which can be collected with satellite-based and ground-based active and passive remote-sensing sensors (Remer et al., 2005; Sundström et al., 2009; Aaltonen et al., 2012; Kolmonen et al., 2013).

Turbulent atmospheric mixing transports gases and aerosol particles of biogenic and anthropogenic origin both within the ABL, and into the free troposphere (Barlow et al., 2011), and thus can have an impact on air quality and processes, such as secondary particle formation (e.g. Janssen et al., 2012; Hirsikko et al., 2013), taking place in the atmosphere. The ABL is also influenced by local topography (e.g. Barlow and Coceal, 2009; Collier et al., 2010). The urban environment is typically composed of roughness elements (buildings and trees) with different heights creating temporally and spatially varying wind and turbulent fields (Wood et al., 2009a); waves and trees induce a similar effect above the ocean and forest, respectively. Thus, characterizing the effect of surface topography and roughness is essential in order to understand the nature of the ABL and processes taking place therein. In addition, buildings and streets enable turbulent mixing in the urban environment even when the rural surroundings are

expected to be quiescent such as during night time (Souch and Grimmond, 2006), and temperature contrasts in coastal areas due to the ocean heat storage generate sea/land breezes (e.g. Gahmberg et al., 2010). Thus, understanding ABL evolution and dynamics in different environments is essential in terms of air quality, climate change assessment and weather forecasting.

The ABL has traditionally been monitored with instruments mounted on low-level (less than 100 m tall) masts, and with associated modelling (van Ulden and Wieringa, 1996; Barlow and Coceal, 2009). Although mast measurements have proven to be valuable for surface-layer meteorological research, mast-based experimental information on ABL evolution is largely missing. However, deployment of sodars and Doppler lidars enables the investigation of ABL wind (e.g. Wood et al., 2009b, 2013a, b) and its turbulent nature from high-resolution vertical velocity profiles (e.g. Hogan et al., 2009; O'Connor et al., 2010; Barlow et al., 2011).

Intensive remote-sensing instrument stations and networks for profiling of the ABL – and tropospheric aerosol particles, clouds and precipitation – have been established by national research and weather service institutes, and in international collaborations (e.g. Illingworth et al., 2007; Flentje et al., 2010; Madonna et al., 2011; Shupe et al., 2013). Previously, a long-term programme, the Helsinki Testbed, was implemented for testing and improving various instruments for weather monitoring and research purposes (Koskinen et al., 2011). Recently, the Finnish Meteorological Institute (FMI), together with the University of Helsinki (UHEL), has established Finland's new ground-based remote-sensing network. The network covers five climatically, environmentally and topographically different locations across Finland, with aims: (i) to provide near-real-time information on the distribution of aerosol particles, and wind profiles in the ABL, for stakeholders such as in now-casting, public information and for aviation safety authorities; (ii) to estimate ABL depths; (iii) to investigate aerosol particles, clouds and precipitation to understand their climate interaction; and (iv) to facilitate interdisciplinary research between atmospheric and ecological sciences.

In this paper, we introduce Finland's ground-based remote-sensing network (Sect. 2), the instrumentation deployed, discuss the measurement strategies at each location and present selected case studies of research potential (Sect. 3). The HALO Photonics Doppler lidars are core instruments in the network. To our knowledge this is the world's first meteorological Doppler lidar network. Therefore, we also focus on the performance of Doppler lidars in challenging environments, by displaying results from two Doppler lidar inter-comparison campaigns performed in Helsinki, discussing the operational reliability (Sects. 4.1–4.2) and presenting case studies (Sect. 4.3). In addition, we discuss the research potential for a network of remote and in situ sensors (Sects. 3 and 4.3).

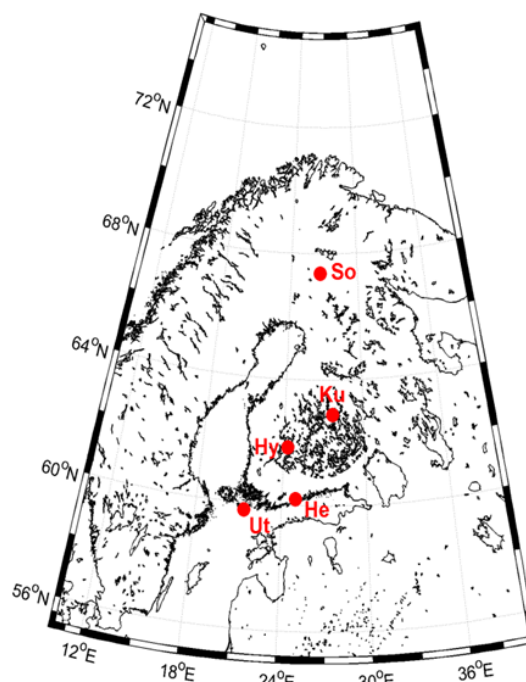


Fig. 1. Map of Finland indicating the network sites: So = Sodankylä, Ku = Kuopio, Hy = Hyytiälä, He = Helsinki and Ut = Utö.

2 Measurement sites

Finland's ground-based remote-sensing network consists of five measurement stations (Fig. 1), which represent a variety of climates, and geological and topographical environments (full details given in Table 1):

1. Helsinki – urban (Sect. 2.1),
2. Kuopio – semi-urban/rural (Sect. 2.2),
3. Hyytiälä – rural (boreal forest) (Sect. 2.3),
4. Sodankylä – arctic rural (Sect. 2.4),
5. Utö – island in Finnish archipelago (Sect. 2.5).

A four-season climate with a harsh winter is common for all stations; average wintertime snow depth is 5–20 cm on the southern coast and up to 80 cm in eastern and northern Finland. The measurement stations have a long tradition in atmospheric ground-based passive remote sensing and in situ observations (Hari and Kulmala, 2005; Engler et al., 2007; Järvi et al., 2009a; Leskinen et al., 2009).

2.1 Helsinki

Helsinki, the capital of Finland, is situated on the coast of the Baltic Sea, with over 1 million inhabitants within the metropolitan area. The coastline is ragged with numerous islands close in, and the city centre abuts the shoreline. The

Table 1. Summary of the measurement sites within Finland's ground-based remote-sensing network: AWS stands for automatic weather station. Doppler lidars are from HALO Photonics. Statistics of the average annual temperature, rain amount and wintertime snow depth are from FMI archive.

Site	Site description	Remote sensing instruments
<i>Helsinki</i> (SMEAR III) 60.20° N, 24.96° E 45 m a.s.l.	Urban environment with inhomogeneous topography, marine and continental influenced climate. Annual average temperature is > 5 °C, average wintertime snow depth is 10–20 cm. Annual rain amount is 900–1100 mm.	1. Doppler lidar (Streamline): since 1 Sep 2011 2. Cloud radar (Mira-35S): test campaign: 8 Sep 2011–31 Mar 2012 3. Ceilometer profiles (CL31): since 22 Jun 2009 4. Three C-band weather radars in research use
<i>Utö</i> 59.77° N, 21.37° E 8 m a.s.l.	Rural island, part of the Finnish archipelago, marine climate. Annual average temperature is >5 °C, wintertime average snow depth is 5–10 cm. Annual rain amount is 900–1100 mm.	1. Doppler lidar (Streamline): since 25 Apr 2012 Ceilometer (CT25K): AWS-cloud base since 15 May 2002
<i>Kuopio</i> Savilahti 62.89° N, 27.63° E 190 m a.s.l. Puijo Vehmasmäki	<i>Savilahti</i> : urban site surrounded by lake and forest. <i>Puijo</i> (SMEAR IV): 75 m tower on top of forest covered hill. <i>Vehmasmäki</i> : rural forest site. Climate is continental. Annual average temperature is 3 °C, average wintertime snow depth is 40–60 cm. Annual rain amount is 900–1100 mm.	1. Raman lidar (Polly ^{XT}): continuous measurements since 16 Nov. 2012 2. Doppler lidar (Streamline until March, 2013, currently Streamline Pro): since 20 Sep 2011 3. Ceilometer profiles (CT25K): since 7 Dec 2009
<i>Hyytiälä</i> (SMEAR II) 61.84° N, 24.29° E 179 m a.s.l.	Rural site surrounded by coniferous forest, continental climate. Annual average temperature is 4 °C, average wintertime snow depth is 40–60 cm. Annual rain amount is 900–1100 mm.	1. Doppler lidar (Streamline): since 14 Dec 2012 2. Ceilometer (CT25K): profiles since 20 Jun 2009
<i>Sodankylä</i> 67.37° N, 26.62° E 171 m a.s.l.	Rural site surrounded by coniferous forest and swamp, sub-Arctic continental climate. Annual average temperature is –2 °C, average wintertime snow depth is 80 cm. Annual rain amount is 300–700 mm.	1. Doppler lidar (Streamline Pro) since Feb 2013 2. Cloud radar (Mira-35S): since 23 May 2012 3. Ceilometer profiles (CT25K): since 20 Jun 2009 4. Microwave radiometers (RPG-2CH-DP, RPG-8CH-DP) since Jan 2013

proportion of forest and park areas increases with distance from the city centre of Helsinki. There are numerous weather and air quality monitoring stations in Helsinki and the surrounding metropolitan area (<http://ilmatieteenlaitos.fi/suomen-havainnot/asema?parameter=4&station=101004>; <http://www.hsy.fi/en/Pages/Default.aspx>). The majority of the research-based atmosphere measurements take place on the Kumpula campus of FMI and UHEL, 4–5 km north-east from the city centre. The campus is surrounded by forest

and buildings to the west and north, and by park, buildings and sea to the east and south. A detailed overview of the surroundings and operation of the Station for Measuring Ecosystem-Atmosphere Relations III (SMEAR III, <http://www.atm.helsinki.fi/SMEAR/>) at Kumpula is given by Järvi et al. (2009a). The station provides continuous measurements of meteorological quantities (e.g. temperature, radiation, wind speed and direction, precipitation), aerosol particle characterization, various trace gas concentrations

and eddy-covariance fluxes (Järvi et al., 2009b, 2012; Nordbo et al., 2012). In addition, an Aerosol Robotic Network (AERONET; Holben et al., 1998) Cimel sun photometer (at 52.8 m a.s.l., above sea level), Vaisala ceilometer CL31 and HALO Photonics Streamline Doppler lidar operate on the roof of the FMI building (44.4 m a.s.l.).

The Doppler lidar is also part of a comprehensive meteorological measurement network, Helsinki Urban Boundary-layer Atmosphere Network (Helsinki Urban Wood et al., 2013b). The main aim of Helsinki Urban is to understand urban meteorological phenomena (Wood, 2010) with the help of continuous measurements from remote sensing (e.g. sodar, scintillometer, Doppler lidar) and in situ instruments. In addition, FMI (and Aalto University) has the capability for airborne in situ observations with a Skyvan airplane, and a Cessna 172, capable of observing atmospheric aerosol particles (Schobesberger et al., 2013) in collaboration with the University of Helsinki, for which regular annual flight campaigns are performed.

2.2 Kuopio

Kuopio is a town with ca. 100 000 inhabitants located in eastern Finland and surrounded by lakes and forests. Remote sensing and in situ measurements are distributed across three locations in Kuopio (Fig. 1):

- Vehmasmäki – rural forest area 18 km from the town centre of Kuopio;
- Savilahti – University of Eastern Finland campus, semi-urban environment;
- Puijo tower – observation tower on a hill covered by coniferous forest.

The multi-wavelength lidar Polly^{XT} – PORTable Lidar sYstem eXTended (see Sect. 3.2) has been deployed continuously at the Vehmasmäki site since November 2012. There is a mast (300 m tall) in the immediate vicinity providing temperature, humidity and wind measurements at numerous levels up to the top. Ground-level aerosol particle measurements at Vehmasmäki include aerosol particle total scatter and backscatter (nephelometer), aerosol absorption/BC (aethalometer) and particle mass.

These measurements are supported by two nearby sites, Savilahti and Puijo tower (SMEAR IV), which are both about 3 km from Kuopio town centre and 2 km separate from each other. SMEAR IV also belongs to the Integrated Carbon Observation System (ICOS, www.icos-infrastructure.fi/) network concentrated on measurements of greenhouse gas concentrations and meteorological quantities. The campus at Savilahti hosts the FMI Kuopio unit in the Melania building, on the roof of which several instruments are installed: a Doppler lidar (HALO Photonics), instruments for measuring aerosol optical thickness (AERONET Cimel sun photometer)

and solar irradiance (direct, diffuse and global; a pyranometer and a Multi-Filter Rotating Shadow band Radiometer). A Vaisala CT25K ceilometer and automatic weather station are located on the ground within 20 m of the building.

The top of Puijo tower is 224 m above lake level (i.e. 306 m a.s.l.), on which instrumentation for aerosol particle size distribution and optical property characterization is installed (Leskinen et al., 2009, 2012). Every autumn, a cloud measurement campaign is conducted at Puijo, since the hill and tower are often inside clouds. The Doppler lidar at Savilahti has the potential for direct line-of-sight scanning above the Puijo tower.

2.3 Hyttiälä

SMEAR II station is in a homogeneous coniferous forest at Hyttiälä. The area around the measurement station is sparsely populated and land use is dominated by forestry and agriculture. Hyttiälä is about 60 km from the nearest town, Tampere (ca. 210 000 inhabitants in 2012). The UHEL-operated station has a long tradition in ground-based in situ measurements (Hari and Kulmala, 2005). The measurement station, its operation and surroundings were introduced in detail by Vesala et al. (1998); therefore, we give only a short description of the current status here.

The measurements include continuous observations of meteorological quantities (e.g. temperature, cloud base height, wind speed and direction), comprehensive aerosol particle physical, optical and chemical properties, trace gas concentrations, gas exchange, water and energy balance (e.g. Manninen et al., 2009; Ilvesniemi et al., 2009, 2010; Launiainen, 2010; Laitinen et al., 2011). Furthermore, measurements are operated in soil, inside and above forest canopy, above the nearby lake Kuivajärvi and Siikaneva wetland. Every spring – during intensive field campaigns – extensive aerosol particle, trace gas and ion measurements are performed (e.g. Kulmala and Tammet, 2007; Williams et al., 2011). Aerosol optical depth is monitored by the Cimel instrument and total ozone column with Brewer MK III spectrometer. The SMEAR II station provides data through AERONET, ICOS, Aerosols, Clouds, and Trace gases Research Infrastructure Network (ACTRIS), Analysis and Experimentation of Ecosystems (ANAEE) and Integrated non-CO₂ Greenhouse gas Observing System (INGOS).

A Doppler lidar (HALO Photonics) was placed on a roof (of the maintenance building) in December 2012, 400 m from the main measurement area where the Vaisala ceilometer is also located. The current location of the Doppler lidar was selected based on the criteria of a stable base, and a clear view for wind profiling and horizontal scanning. In the future, it is possible that the Doppler lidar will be moved closer to the other measurements when the construction of a new sturdy tower has been completed.

2.4 Sodankylä

The Arctic Research Centre (ARC, <http://fmiarc.fmi.fi>; Kivi et al., 1999) of FMI is located 7 km from the centre of the town Sodankylä (ca. 5500 inhabitants) and is situated north of the Arctic circle (Fig. 1). The centre has been constructed on the bank of the river Kitinen, and is surrounded by coniferous forest dominated by pine trees. Much of the land nearby is a large bog. An infrequently operated airport (light aircraft, gliders and helicopters) is located 4 km north of ARC.

A Doppler cloud radar (Metek GmbH) has been installed close to the radiosounding station and next to MARL (Mobile Aerosol Raman Lidar) of the Alfred Wegener Institute for Polar and Marine Research (AWI), Germany. Manual balloon-borne soundings of ozone are performed weekly at the sounding station, together with other less-frequent special soundings including water vapour and aerosol particle properties. Radiosoundings for vertical profiles of meteorological quantities are carried out twice a day by a Vaisala Automatic Sounding Station. In addition, the site also gathers automatic synoptic weather observations. The sounding-station roof, and a 16 m tower beside it, accommodates a Vaisala CT25K ceilometer, Doppler lidar (HALO Photonics) and radiation sensors (including spectral measurements in the UV range, global, reflected, diffuse and direct components of solar radiation). Total ozone column is measured with a Brewer MK III spectrometer, aerosol optical depth is observed with Precision Filter Radiometer (PFR) and CO₂ and CH₄ columns are measured with Fourier Transform Spectrometer. A recent investment was made in a Cimel instrument with an additional cloud-mode feature which enables investigation of cloud optical properties through AERONET (Chiu et al., 2010).

There is a meteorological mast 500 m south of the sounding station, providing temperature, humidity and wind speed at 3, 8, 18, 32, 45 and 48 m. Surface-layer turbulence is estimated with sonic-anemometer eddy-covariance measurements at heights of 25 and 48 m. Fluxes of water vapour and carbon dioxide are calculated from CO₂/H₂O gas analysers which are co-located with the sonic anemometer. Snow depth, soil temperature and soil respiration measurements are carried out next to the mast.

2.5 Utö

The island of Utö (Fig. 1) is on the outer edge of the Finnish archipelago in the Baltic Sea, 60 km southwest from the mainland and about 10 km from the next nearest island of similar or larger size. The 1 km² island is a background site whose air quality is influenced regularly by nearby ship traffic (Hyvärinen et al., 2008). The sea around Utö is ice-free almost year-round except in the direction of the archipelago (north), which can be covered by ice for 1 or 2 months. The ground is rocky and partly covered by underbrush. The island has about 50 year-round inhabitants.

FMI performs a wide range of atmospheric observations in Utö. Due to its location beside the main ship tracks, monitoring of the weather has a long tradition on the island. These observations include temperature, wind speed, direction, visibility and cloud-base height. Engler et al. (2007) introduced continuous ground-based in situ aerosol particle observations in 2003. In addition, Utö is a member of the ICOS network. Measurements within ICOS include monitoring of greenhouse gas concentrations and meteorological quantities. Recent investments at Utö include a Doppler lidar (HALO Photonics) and a comprehensive sea gas flux and wave observation station. The greenhouse-gas-monitoring station operates on the northern side of the island (Enskär). Sea gas flux and wave measurements are carried out west of cape Kesnäs, and aerosol particulate, Doppler lidar, ceilometer and other operational weather observations are made on the eastern side of the island (Österäng). The Doppler lidar is placed on top of an old measurement container (ca. 8 m a.s.l.) and has an almost uninterrupted view down to low elevations in every direction except for the lighthouse on the island (northwest direction).

3 Instrumentation

The development of Finland's ground-based remote-sensing network has been progressed step by step (Table 1): (i) by deploying the Helsinki weather radar network, which is a joint co-operation between FMI, UHEL and Vaisala Inc., (ii) by utilizing the existing ceilometer network and starting backscatter profile collection in Helsinki, Kuopio, Hyytiälä and Sodankylä in 2009, (iii) by installing three Streamline Doppler lidars in 2011, (iv) by installing a scanning cloud radar and two Doppler lidars in 2012 and 2013, and (v) starting ceilometer backscatter-signal collection in Utö in the future. In addition, there is one spare Doppler lidar to provide a drop-in replacement for the network lidars during maintenance or malfunction (rather than lying idle, various research campaigns are planned for the spare lidar). We now give a description of each remote-sensing instrument (Table 2).

3.1 Doppler lidar

FMI has five network, and one spare, pulsed Doppler lidars from HALO Photonics (<http://halo-photonics.com/>, Pearson et al., 2009). The backscatter return of the pulsed 1.5 μm wavelength signal is observed with a heterodyne detector (Table S1 in the Supplement). The Doppler lidar measures the backscattered signal in co- and cross-channels which allows determination of the depolarization ratio of scattering targets. The Doppler lidars are equipped with built-in heating and cooling systems. In addition, the lidar lens and calibration plate are heated to minimize snow and ice build-up.

FMI has two types of Doppler lidars (four Streamline and two Streamline Pro model lidars), whose characteristics are

Table 2. Summary of measured quantities and means of application (with example references) of remote-sensing instruments: β and Z_e refer to attenuated backscatter coefficient and radar equivalent reflectivity factor, respectively.

Instrument (targets)	Measured parameters	Applications
<i>Doppler lidar</i> (aerosol particle, cloud droplets, ice crystals, snow, precipitation)	Radial profiles of β (co- and cross-channels), Doppler velocity, SNR	Water cloud base height and dynamic studies, aerosol particle depolarization ratio and dispersion (this paper), mixing layer height (O'Connor et al., 2010), wind profiles (Henderson et al., 2005), 2–3-D wind field (Wood et al., 2013a)
<i>Polly^{XT}</i> (aerosol particles, cloud droplets, water vapour)	Vertical profiles of the particle β at 355, 532 and 1064 nm, β at 532 nm (cross-polarized) and extinction coefficient at 355 and 532 nm, water vapour at 407 nm	Ångström exponents at 355 and 532 nm and linear/aerosol particle depolarization at 532 nm, particle surface area, volume, effective radius, refractive index and single scattering albedo at 532 nm, water vapour mixing ratio (Sect. 3.2)
<i>Cloud radar</i> (cloud droplets and crystals, snow, precipitation and drizzle)	Z_e (co- and cross-channels), Doppler velocity, spectral width, SNR	Cloud-top height and ice water content (CloudNet; Hogan et al., 2006), cloud vertical dynamics, 3-D cloud imaging when scanning, linear depolarization ratio (measurement software provided)
<i>Ceilometer</i> (aerosol particle, cloud droplets and crystals, snow, precipitation)	Vertical profiles of β , cloud-base height	Cloudiness, aerosol layer heights (several methods available; e.g. Haeffelin et al., 2012; Emeis et al., 2008)
<i>Weather radar</i> (precipitation, snow)	Z , Doppler velocity, Doppler spectral width	Linear depolarization ratio, precipitation target categorization, precipitation rate and accumulated amount, wind speed and direction (Sect. 3.4)
<i>Sodar</i> (turbulent fluctuations)	Vertical velocity profiles	Shallow (< 400 m) ABL depth from vertical velocity and wind profile
<i>Microwave radiometer</i> (water vapour)	Brightness temperature	Profiles of temperature and humidity (e.g. Cimini et al., 2006)

identical apart from their scanning capabilities and receiver sensitivity. The Streamline model Doppler lidars are capable of full hemispheric scanning. The recent Streamline Pro models have no external moving parts, with the scanning head mounted inside the lidar case. This limits the scanning to within a 20° cone around the zenith. According to the manufacturer, the Pro model has a narrower receiver frequency bandwidth and therefore it should be more sensitive, which makes it more suitable for arctic conditions.

The Doppler lidars operate with a pulse repetition frequency of 15 kHz, pulse length of 200 ns, and initial data points are oversampled at 3 m resolution. Ten points are then combined to give a final spatial resolution of 30 m, with a total of 320 gates out to a radial distance of 9.6 km. The temporal resolution can be as fast as 1 s. However, to obtain good sensitivity in the clean air at northern latitudes, it is necessary

to integrate for longer times; usually 15–30 s. Useful signals are limited by the presence of reasonable aerosol load. Typically, this means measurements only in the ABL with vertical limits varying from 0.4–1 km, depending on season, and from 1–4 km when scanning near horizontal. Liquid water, mixed phase and ice clouds can be detected out to the maximum 9.6 km detection range.

Continuous vertical staring and a three-beam Doppler beam swinging (DBS) wind profile measurement every 10 min are standard operation modes for the FMI Doppler lidars. In between the operational tasks, custom-designed scanning is performed. To date, a variety of vertical azimuth display (VAD) and range height indicator (RHI) strategies have been deployed in Utö (see Sect. 4.3) and Helsinki. Similar strategies are planned to be performed with the remaining two full hemispheric scanning lidars.

As standard, the Doppler lidar provides profiles of signal-to-noise ratio (SNR), uncalibrated attenuated backscatter coefficient (β) and radial Doppler velocity (v). Post-processing then applies background and focus corrections to the signal and provides calibrated attenuated backscatter coefficient profiles, together with uncertainties in signal, attenuated backscatter and Doppler velocity derived using an approximation to the Cramér–Rao lower-bound method (Rye and Hardesty, 1993) given in O'Connor et al. (2010). Data availability is determined based on SNR (after applying the background correction); the threshold being determined based on the acceptable uncertainty for a given application. For vertically pointing data, our selected threshold of -21 dB for SNR is equivalent to an uncertainty of about 0.05 m s^{-1} for the Doppler lidar instrument. Lowering the threshold to -25 dB theoretically only increases the uncertainty to 0.1 m s^{-1} , potentially still suitable for horizontal wind measurements, but may then be within the noise floor of the instrument. Data affected by clouds or precipitation are not flagged by default.

The Doppler lidar attenuated backscatter coefficient can additionally be calibrated according to a procedure introduced by O'Connor et al. (2004). In this method, the integration of attenuated backscatter, β , from a nearly non-drizzling cloud base through to infinity is set equal to $1/(2\eta S)$, where η is the multiple scattering factor and S is the lidar ratio. Both η (close to 1) and S (20 sr) are assumed to be constant and known for this lidar wavelength in stratocumulus clouds (Westbrook et al., 2010a). A non-drizzling condition 250 m below the cloud base is determined by requiring backscatter coefficient values to be smaller than a certain threshold value, namely 10 times smaller than the backscatter coefficient inside liquid cloud (O'Connor et al., 2004). If the telescope focus length is changed (see Sect. 4.1), a new calibration should be calculated. The uncertainty in the calibration method is 20 %.

The measurement software does not provide depolarization ratio. In our signal processing we calculate the depolarization ratio as a ratio of the backscattering signal from the cross-polar channel to the co-polar channel (i.e. $\delta = \beta_{\perp}/\beta_{\parallel}$). We do not yet employ any calibration procedure for the depolarization ratio or Doppler velocity. The performance of the Doppler lidar for aerosol depolarization profiling (e.g. backscatter and depolarization) will be determined through comparison with the Raman lidar Polly^{XT} introduced in Sect. 3.2.

Wind profile data are measured using the three-beam DBS technique, in which one vertical beam, one northward beam and one eastward beam are measured. The northward and eastward beams are tilted 15 – 20° from the zenith. Wind speed and direction are calculated using trigonometry and assuming that no major changes occur within the DBS volume (Henderson et al., 2005; Lane et al., 2013). Custom scanning data require different methods to provide more sophisticated

information on ABL wind and dynamics (e.g. Banta et al., 2006; Wood et al., 2013a).

3.2 Raman lidar

The lidar at Vehmasmäki ($62^{\circ}44'17''$ N, $27^{\circ}32'33.5''$ E, 190 m a.s.l.) is a seven-channel Raman lidar Polly^{XT} (Table S2 in the Supplement; Althausen et al., 2009; Engelmann et al., 2012). Polly^{XT} provides vertical profiles of the particle backscatter coefficient at 355, 532 and 1064 nm, and the particle extinction coefficient at 355 and 532 nm. The Raman method (Ansmann et al., 1992) is deployed to retrieve backscatter coefficients and extinction at 355 and 532 nm. The relative statistical error is typically $< 5\%$ for the backscatter coefficients and $< 10\%$ for the extinction coefficients. For the backscatter-coefficient profiles at 1064 nm and within the troposphere, the Klett method (Klett, 1981) is used assuming height-constant lidar ratios. An overlap correction following Wandinger and Ansmann (2002) is deployed. We use a threshold value 0.7 for the overlap correction which allows data starting from 500 m or even lower. Columnar aerosol optical depth can be estimated from the integrated extinction coefficients with the assumption of a constant extinction for the first 500 m. The vertical resolution is 30 m and currently raw data are stored as 30 s averages.

Intensive particle quantities such as the Ångström exponents, the lidar ratio at 355 and 532 nm and linear particle depolarization at 532 nm can be analysed. The top height and the evolution of the ABL and night time residual layer can be defined together with the macrophysical properties (i.e. height and thickness) of cloud and aerosol layers (Fig. 2). The depolarization channel (532 nm) can be used to diagnose the phase of water; spherical water droplets have a depolarization ratio just above 0 % and complex ice crystals about 40 %. Other particulate types, such as dust, also have characteristic depolarization ratios through which they can be identified. The depolarization measurements are calibrated by following Freudenthaler et al. (2009). A controllable rotary mount with polarizers close to the focal plane of receiver telescope is installed in the system. The polarizer is rotated $+45$ and -45° with respect to the laser polarization plane in the light path. This makes it possible to retrieve the volume linear depolarization ratio from the signal ratio of the cross-polarized and the total channel, and obtain calibration constants (Freudenthaler et al., 2009). The calibration measurements are performed three times a day. The system also includes a water-vapour channel (407 nm) (Engelmann et al., 2012). With continuous measurement of aerosol particle backscatter, extinction, depolarization and water vapour mixing ratio, the lidar is suitable for cirrus cloud and aerosol particle studies – as well as for stratospheric observations during night time.

In the example measured on 31 March 2013, two pronounced layers were identified. First, the ABL evolution in the lowermost 2 km, where aerosol particles were well

mixed, can be followed. Second, the evolution of an elevated aerosol particle layer was observed within the free troposphere, at around 7–8 km altitude (Fig. 2). Aerosol particle depolarization ratio (Fig. 2) was rather low for this layer, and hence indicates the presence of spherical, i.e. more-aged or hydrophilic, particles. The water-vapour measurements showed enhanced relative humidity within the ABL, while the elevated aerosol particle layer was drier. The example from 31 March 2013 shows how the Polly^{XT} Raman lidar can be used for tropospheric aerosol particle studies of the ABL (Korhonen et al., 2014), the characterization of elevated tropospheric aerosol particle layers, for water-vapour profiling and continuous long-term monitoring (Komppula et al., 2012). Compared to Doppler lidar, the Polly^{XT} is more sensitive to elevated aerosol particle layers and the independent determination of backscatter and extinction profiles allows the calculation of microphysical properties of aerosol particles when inversion methods are used (Althausen et al., 2009). Indeed, Doppler lidar aerosol attenuated-backscatter profiles were available up to 400–500 m during the period 06:00–10:00 UTC on this day, whereas the air was too clean for sufficient data quality during the rest of the day. A combination of water-vapour and aerosol particle microphysical retrievals from Polly^{XT}, together with mixing layer evolution and winds from a Doppler lidar, enables a more comprehensive and detailed investigation of the aerosol particles, their fluxes (Engelmann et al., 2008) and the ABL than from either instrument alone.

Microphysical data of non-polarizing particles can be derived with inversion algorithms. By following the method developed at the Leibniz Institute for Tropospheric Research (Müller et al., 1999), estimates can be made for particle surface area, volume, effective radius, refractive index and single scattering albedo at 532 nm. Uncertainties in the retrievals are estimated according to Müller et al. (1999) to give an uncertainty for effective radius of < 30 %, and for volume and surface area concentration of > 50 %. The maximum uncertainty of the real part of the complex refractive index is ± 0.1 . When the imaginary part is $> 0.01i$ the uncertainty can be as high as 50 %. The accuracy of single-scattering albedo estimates depends on uncertainties in the optical data.

Polly^{XT} has been part of the European Aerosol Research Lidar Network (EARLINET; Bösenberg et al., 2003) since 2012. The objectives of EARLINET are reached by operating a network of, presently, 23 stations distributed over Europe using advanced quantitative laser remote sensing to directly measure the horizontal, vertical and temporal distribution of aerosol particles. Special care is taken to assure data quality, including instrument inter-comparison. A major part of the measurements is performed according to a fixed schedule to provide an unbiased and statistically significant data set. Additional measurements are performed to specifically address temporally or spatially limited aerosol events.

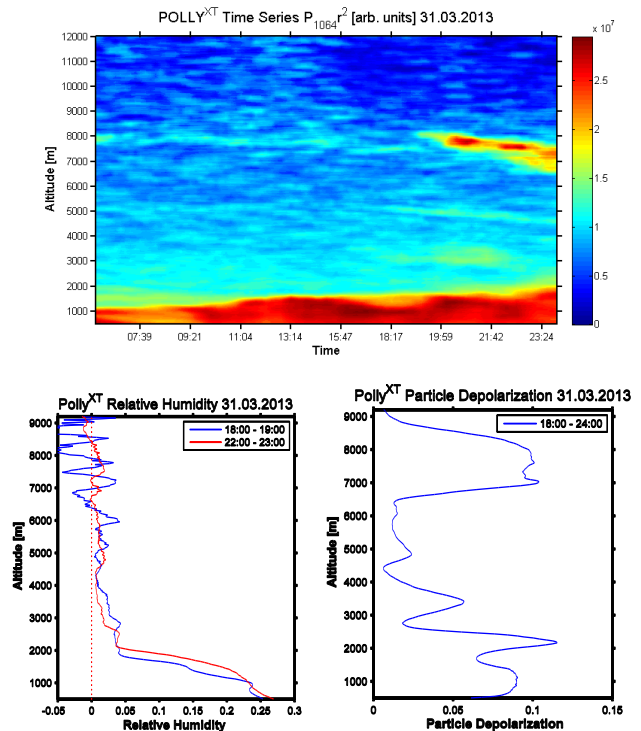


Fig. 2. An example of the range-corrected signal at 1064 nm (top panel) of the Polly^{XT} lidar in Vehmasmäki on 31 March 2013. Lower-left panel, 1-hour average relative-humidity profiles; lower-right panel, 4-hour average particle depolarization ratio profile.

The lidar is mounted in a container, which has a glass window on the top, in order to prevent hazardous effects of ambient temperature changes and snowfall. The operation of the Raman lidar is planned to be continuous in Vehmasmäki. However, in the case of precipitation, the measurements are stopped automatically. The device is portable and it can be transported, e.g. in the case of a volcanic eruption, to detect aerosol plumes.

3.3 Cloud radar

The MIRA-35S (metekgmbh.dyndns.org) is a full-hemispheric scanning Doppler Cloud radar (Görsdorf et al., 2011). In order to detect clouds, a high sensitivity is required. The reflectivity of visible clouds is in the range -70 to -20 dBZ, the reflectivity of rain droplets is in the range $+15$ to $+60$ dBZ; and the reflectivity of drizzle below clouds is in the reflectivity range between values from cloud and precipitation. The cloud radar is optimized to be sensitive to cloud and drizzle droplets at short range (up to 30 km) with fine spatial resolution (typically 30 m). For comparison, weather radars provide large range coverage (up to 150 km around the radar) with sufficient sensitivity for detecting rain (see Sect. 3.4). Compared to lidars, the

extinction of the radar signal in non-precipitating clouds is negligible.

The cloud radar is based on a 35 GHz magnetron transmitter providing short pulses with high pulse power which allows a range resolution of 30 m and sufficient sensitivity for most visible clouds (see Table S3 in the Supplement for technical details). Typically a pulse repetition frequency (PRF) of 5 kHz is used, which allows a maximum range of 30 km and a velocity range of $\pm 10.6 \text{ m s}^{-1}$. The radar signal is converged by a Cassegrain antenna having 1 m diameter and beamwidth of 3 dB (equivalent to 0.56°). From the down-converted receiving signal of each range gate, Doppler spectra are calculated using a 512-point fast Fourier transform (FFT). One profile of spectra is calculated from the signal of 512 successive pulse cycles (0.1024 s). Typically 100 spectra (10 s) are averaged to increase the statistical significance and sensitivity of the Doppler spectra. After removing the receiver noise from the averaged spectra, the first three moments (reflectivity, Doppler velocity and Doppler spectrum width) are calculated from the peaks identified in the spectra. The cloud radar transmits using vertical polarization (if the beam is pointing horizontally), and simultaneously receives in both the vertical and horizontal polarization channels, hence providing linear depolarization ratio (LDR).

The system can save raw data or un-averaged spectra, but normally only 10 s-averaged spectra are saved (30 GB day^{-1}). The spectra are routinely converted to a compressed format, thus saving only the spectral bins containing signal. Depending on the amount of clouds, these files typically occupy about 100 MB day^{-1} . The measurement strategy of the cloud radar has been to point vertically and gather good-quality data within 14 km.

Insects cause strong signals in the ABL. These signals can be recognized because they have high LDR values and because they are below the melting layer where the hydrometeors have very low LDR values. These signals are filtered in such a way that, for each range gate, one set of moments for the insects and one for the hydrometeors are saved.

Cloud radar observations alone provide a useful basis for cloud research (e.g. Tonttila et al., 2011), however, the sensitivity of cloud radar to low-level liquid clouds can be limited. Cloud radar is a key instrument in multi-sensor synergetic retrievals and analysis of clouds. As an example, CloudNet (a network of stations for the continuous evaluation of cloud and aerosol profiles in operational NWP models) developed a scheme to quantitatively analyse cloud types, microphysical properties of ice clouds and drizzle flux, and cloud fraction, by combining data from a microwave radiometer, ceilometer, cloud radar with radiosonde or model profiles of temperature and humidity (Illingworth et al., 2007). This scheme will be implemented at Sodankylä within the ACTRIS framework. In addition, the inclusion of Doppler-lidar observations allows the investigation of cloud-base and below-cloud dynamics, and to identify whether clouds are coupled to or decoupled from the surface (Hogan et al., 2009; Harvey et al.,

2013). When clouds are coupled with the surface, the inclusion of in situ observations in the analysis is justified.

3.4 Helsinki weather-radar network

The Helsinki metropolitan area hosts three dual-polarized C-band weather radars. One of them, Vantaa weather radar (VAN), belongs to FMI and is deployed for operational applications (Saltikoff and Neuvonen, 2011). The Kumpula radar is located in Kumpula campus of the UHEL and is operated by the Department of Physics. The third radar is a research and development radar of Vaisala Inc. and is used for research purposes by the UHEL radar meteorology group. The Helsinki weather radar network is deployed to study high-latitude precipitation and its impact on quantity and quality of storm water, and it acts as one of the ground validation sites for the upcoming NASA Global Precipitation Mission (Hou et al., 2008).

The current operation strategy includes synchronized scans at low-elevation angles. Since the Vantaa radar operation schedule is fixed, Kumpula and Kerava radars perform low-elevation scans with a similar system setting to that of Vantaa radar every 15 min. An example of a joint retrieval is presented in Fig. 3, where snowfall rate is estimated by using the FMI operational snowfall-rate reflectivity relationship (Saltikoff et al., 2010) that was applied to the three-radar maximum-reflectivity composite. In Fig. 3b and c dual-Doppler wind speed and direction, calculated from Doppler velocity measurements, are shown.

Given the greater flexibility of the research radars, their operation schedule is adopted to current research interests. Juga et al. (2012) analysed Vantaa and Kumpula radar observations to investigate the cause of a large traffic accident. Vantaa radar observations were supplemented by the vertical scans of Kumpula radar that provided a vertical structure of the precipitation field. Research, however, is not limited to pure meteorological applications; Leskinen et al. (2011) for instance reported an application for monitoring pest insect immigration.

One of the current plans related to the Helsinki radar network is to upgrade it to distributed collaborative adaptive sensing (DCAS) capabilities (McLaughlin et al., 2009). This will be achieved by adding a fourth radar, which, together with the Kumpula and Kerava radars, will form a DCAS network, where scanning strategies will be adaptively modified depending on weather conditions.

3.5 Ancillary remote-sensing observations

Ancillary remote-sensing instrumentation includes a Vaisala 905 nm wavelength ceilometer at each station (Vaisala, 1999). Traditionally, the ceilometer network has been utilized for cloud-base detection and cloud-cover monitoring in Finland. Furthermore, the ceilometers have collected aerosol particle backscatter profiles in Sodankylä, Kuopio, Helsinki

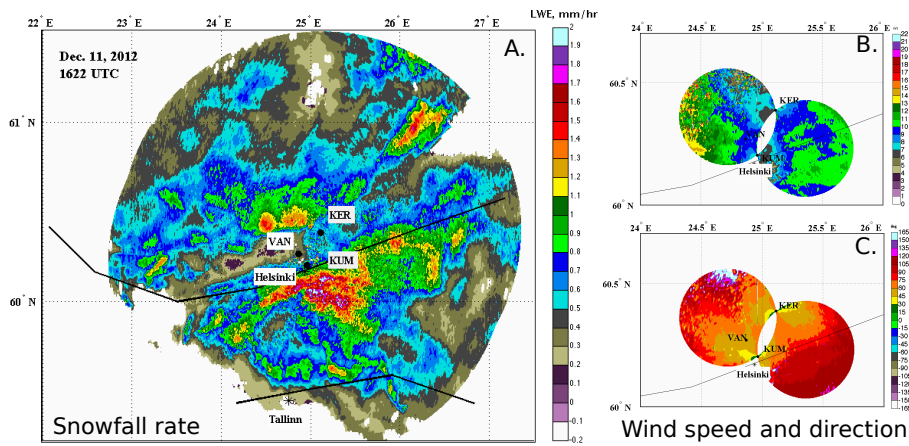


Fig. 3. Helsinki weather radar network observations: (a) precipitation (snowfall) rate as measured by the three radars, (b)–(c) dual-Doppler wind speed and direction estimated from Kumpula and Kerava radar observations.

and Hyytiälä since 2009 (Table 1). Aerosol particle profiles have also been deployed to investigate ABL evolution (e.g. Milroy et al., 2011). Each station, excluding Utö, has a Cimel or Precision Filter Radiometer sun photometer to monitor columnar aerosol optical properties (Aaltonen et al., 2012). We installed a new Cimel instrument with additional cloud optical-depth mode (Chiu et al., 2010) at Sodankylä in March 2013.

At Sodankylä, a seven-channel Raman lidar MARL (Immeler et al., 2008), which is used to retrieve vertical profiles of cloud and aerosol particle properties, as well as water vapour profiles, is operated close to the sounding station. MARL was installed at Sodankylä in September 2010. Since then the instrument has been operated by FMI in cooperation with the AWI. The instrument was built in 1996 and it is owned by the AWI. It measures backscatter coefficients (co- and cross-polarized) and extinction coefficients at 355 and 532 nm, and water vapour mixing ratio. It is mainly suited for higher tropospheric and stratospheric profiling.

Since January 2013, two Microwave radiometers (Radiometer Physics GmbH) have provided atmospheric brightness temperatures. Sodrad1 (RPG-8CH-DP) measures at 10.65, 18.7, 21, 37 GHz and Sodrad2 (RPG-2CH-DP) measures at 90 and 150 GHz (Rose and Czekala, 2009). A five zenith angle (0, 48, 60, 66 and 71°) scanning routine with 20 s integration in each direction has continuously been applied.

4 Doppler-lidar performance

The strategy behind Finland's new remote-sensing network is to co-locate an additional advanced instrument, such as a Raman lidar, cloud radar or weather radar, with each Doppler lidar, where possible. Therefore, in this section we concentrate on evaluating the performance of the Doppler lidar and applicability via case studies. In Sect. 4.1 Doppler

lidar operational reliability and challenges in Finland are discussed. In addition, results are introduced from two Doppler lidar inter-comparison campaigns which were performed at Helsinki after the instruments had arrived from the manufacturer (Sect. 4.2). The aim was to investigate the performance and inter-comparability of the Doppler lidar wind and backscatter signal profiles before deployment within the network. In Sect. 4.3 the potential research applications for the Doppler lidar network are introduced.

4.1 Doppler-lidar operation reliability and limitations in Finland

4.1.1 Observation limitations due to ambient conditions

The Doppler lidar backscatter coefficient is proportional to $\sim nd^{1-2}$, i.e. target number concentration (n) and diameter (d) to power 1–2 depending of wavelength (Weitkamp, 2005; Henderson et al., 2005). Particles larger than 0.1λ in diameter, where λ is the scattered wavelength, scatter light according to Mie theory. Thus, Doppler lidar signal return is dominated by particles larger than 150 nm in diameter, while backscatter from air molecules is negligible at this wavelength.

Ambient aerosol particle number concentration and mass is low or moderate at the network stations (e.g. Kulmala et al., 2001; Engler et al., 2007; Dal Maso et al., 2008; Leskinen et al., 2009), apart from Helsinki (Aarnio et al., 2005; Hussein et al., 2007). Therefore, it quickly became clear that special attention would be required for the setting up of measurements: since signal below the noise threshold (i.e. -21 dB) was frequent and, vertically, the length of line of sight was often only couple of hundred metres. Changing the telescope focus length from infinity to 1–2 km has helped the collection of more data within the ABL, as one could expect (Fig. S1 in the Supplement). The Doppler lidars have built-in software-controllable motors to change the

telescope focus length, and, for the newest Doppler lidars (one Streamline and both Steamline Pro models), there is a software update which enables adjustment of the telescope focus separately for each task, i.e. one focus for vertical stare and one for horizontal scanning. We consider that there is no universally optimal telescope focus setting for these Doppler lidars, but it rather depends on the measurement environment and purpose of observations. We are interested in representative ABL observations in environments having low aerosol particle concentration, and therefore, a short telescope focus length is optimal within the Finnish network. Currently, the standard operational setup is for the telescope focus to be set to 1–2 km for ABL applications, while low-elevation scans are performed with the focus set to infinity.

Changing the telescope focus is not always sufficient. To increase data sensitivity, it is also necessary to increase the integration time. The instrument has user-selectable temporal resolution. One ray is then defined as a single profile obtained by accumulating all available pulses within the time period selected. Thus, given a selected time resolution of 5 s, and a pulse repetition rate of 15 000 Hz, one ray is obtained from the accumulation of 75 000 pulses. Computation of the velocities is performed in real time. Additional integration across a number of rays can then be used to increase the sensitivity. This method of ray integration allows a simple method for different scan sequences to accumulate across separately specified multiples of the selected temporal resolution; e.g. vertical stare recorded at 5 s resolution and wind measurements recorded at 20 s resolution. Selected temporal resolution and ray integration is dependent on the site, since a humid marine location does not require the same sensitivity as a clean-air Arctic location for the derivation of winds.

Initially, quite low temporal resolution was selected, with as much as 30 s (450 000 pulses) per ray to attempt to gain enough sensitivity to measure up to 2 km. However, despite these attempts, there were not enough aerosol particles to provide a return signal above the ABL, which can be very low in Finland. Additionally, the aerosol present within the ABL may also be insufficient to provide a reasonable return signal, even after extensive averaging. This is especially true for the cross-channel, where the signal is typically too low to confidently calculate a depolarization ratio for aerosol particles. In Sect. 4.2.2 we concentrate only on measurements with 10 s integration from the first inter-comparison period.

Additionally, the detection range of ABL wind profiles derived from DBS data measured in Kuopio during 1 year (20 September 2011–20 September 2012) was analysed. Based on 23 092 wind profiles observed during cloud-free conditions, the maximum detection range was 2340 m a.g.l. and the average range was 400 m (± 1 standard deviation 250 m) above ground level. The near-horizontal detection range has been checked in Helsinki and Utö, where good quality (i.e. SNR > -21 dB) data have been collected up to 4.5 and 1.5 km, respectively. It is clear that, during rain

or snow, the lidar signal is attenuated and the penetration distance depends on the amount of precipitation.

4.1.2 Effect of temperature and weather

FMI operates the Doppler lidar network continuously throughout the year. Thus, reliable operation in all weather conditions is preferable. Finnish winter weather often sets special requirements for measurement devices. The Doppler lidar performance was tested by the manufacturer in a cold room at temperatures down to -20°C , and the first harsh winter when the Streamline lidar was operated continuously in Finland during winter 2011–2012, ambient temperatures reached a low of -26°C in Helsinki. Subsequently, the Streamline Pro model (with no external moving parts) was installed at Sodankylä, where temperatures are regularly below -30°C . Based on this experience, it can be stated that the instrument operation is not unduly affected by low ambient temperatures, due to sufficient insulation and the built-in heating system. The temperature inside the instruments was always above 7°C and only the computer graphical interface was slower than usual.

However, accumulation of snow on top of the Doppler lidar can cause issues. The first concern is the mobility of the scanning head when snow or ice accumulates on it. Based on experience, the accumulation of a 30 cm deep layer of soft snow does not cause scanner mobility problems. However, formation of ice from melting snow or super-cooled water has been observed to stop all scanning motion. On these occasions, the instrument software disengages the scanning motors to avoid damage. The only disadvantage is that measurements may still continue, and scheduled scanning tasks be apparently completed. The second concern is related to accumulation of snow and ice on the lidar lens, since both attenuate the lidar signal (Fig. 4). The amount of signal attenuation depends on the volume, and formation of thick snow and ice layers can attenuate the signal completely (Fig. 4). The internal heating is usually sufficient to remove light snow and rain, but frequent maintenance in icing conditions is required, since no warning flags are available.

The Streamline Pro lidar model was designed for Arctic (i.e. low aerosol particle content) and harsh winter conditions. The new Pro model was tested in real winter conditions in Helsinki, Kuopio and Sodankylä for the first time during winter 2012–2013. With the help of an additional blower, the slanted window is kept relatively clean from water droplets and snow. However, manual cleaning is still required during heavy snowfall.

4.2 Comparison of measurements

Data quality and reliability of measurement devices should be known and tested before beginning operational observations. Therefore, two inter-comparison measurement campaigns were conducted in Helsinki with the aim of comparing

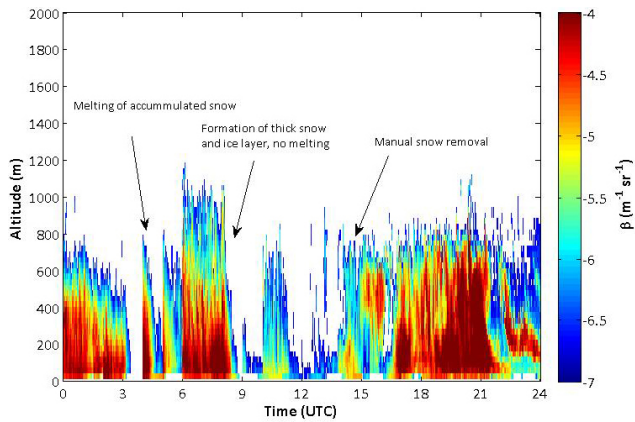


Fig. 4. Effect of snow on Doppler lidar attenuated backscatter profiles in Helsinki on 4 February 2012. Snowfall rate was reasonably constant throughout the day, according to weather radar observations.

profiles of the attenuated backscatter coefficient, and horizontal wind speed and direction (Sects. 4.2.1–4.2.2). In addition, single range gate wind velocity data were compared against in situ sonic anemometer data from SMEAR III, and at SMEAR IV (Sect. 4.2.3).

4.2.1 Measurement setup during inter-comparison campaigns

An intensive inter-comparison campaign was performed with three Streamline Doppler lidars (production numbers 32–34) side by side on a large concrete slab on the roof of the FMI building in Helsinki (Table 3) in September 2011. During this measurement period each instrument was configured to have the same settings: telescope focus length, data integration time, spatial and temporal resolution (Table 3). The scan schedule selected was vertical stare interspersed with a DBS wind profile every 10 min. The temporal resolution for all rays was 10 s (150 000 pulses) and the timing of the wind profile scan was deliberately not synchronized between Doppler lidars. A three-beam DBS scan was selected, which took 30 s to complete each of three profiles with a ray having the same 10 s resolution as the vertical stare.

The second inter-comparison campaign was carried out during winter of 2012–2013 (Table 3). The two Streamline Pro model Doppler lidars (production numbers 53–54) were operated next to a new Streamline model (no. 46) on the roof of the FMI building in Helsinki, with one of the original Streamline models (no. 34) in operation 100 m away on the other side of the roof. Operational parameters for this campaign are presented in detail in Table 3. During the second campaign, vertical-stare data were realized using 6 s integration, while 4 s integration was applied for each ray in the three-beam DBS wind scan. The wind profiles were collected every 3 min, and, again, the timing of the DBS scans were not synchronized between lidars. In addition, the effect

of the telescope focus length on data quality was investigated (see Table 3 for details). During the second campaign the measurements were hampered by nearly continuous rain and snow, and profiles affected by these were excluded from the wind analysis.

4.2.2 Inter-comparison of signal, attenuated backscatter coefficient and wind profiles

The primary measurements are SNR and radial Doppler velocity. The instrument software calculates the background noise to output SNR from the signal power. The internal background-noise correction was first checked to see if it was correctly derived and applied; this was the case for all three instruments in the first inter-comparison period. Next, the SNR profiles were compared. The uncertainties at each range gate can be derived from the instrument parameters (O'Connor et al., 2010) and each instrument conformed closely to the theoretical expectation. Since all instruments were set to have the same telescope focus, it was expected that the SNR profiles would have the same shape. Slight differences in laser energy output and other internal losses in the fibre optic cable, amplifier and telescope optics should then result in a scale offset which would then be compensated for when applying a calibration factor. Range correction using the telescope function for the given focus, and appropriate scaling factor for the laser energy, then allows the provision of the attenuated backscatter profile (Weitkamp, 2005). The initial comparison between SNR profiles from each instrument showed that Doppler lidars 32 and 33 agreed with each other, and had very similar offsets; in essence they had the same calibration factor. Instrument 34 did not agree until it was realized that the stated telescope focus for this instrument was incorrect. Figure 5 shows the resultant range-corrected profiles in arbitrary units, first assuming that all instruments have their telescope focus set to infinity. An appropriately scaled co-located ceilometer profile is also shown. This scaling is necessary since aerosol backscattering is not expected to be similar at the two disparate wavelengths. Profiles from Doppler lidars 32 and 33 agree with each other and the less sensitive ceilometer (note the increased noise in the ceilometer profile). Doppler lidar 34 clearly has an incorrect focus. After using the correct focus, determined to be about 1000 m, the profile shape agrees with the other instruments. In addition, this instrument was noted to be about 25 % more sensitive than the other two, which is then reflected in the calibration factor applied to this instrument. The focus correction was then checked by scanning close to horizontal. In ideal conditions, consisting of homogeneous aerosol in the boundary layer, this provides an additional method for checking that the focus is as stated. Unfortunately, the urban location bordering the Baltic Sea in Helsinki means that such conditions are not that common and such assumption may be unreliable. Since modifying the telescope focus has a major impact on the sensitivity at further ranges, an incorrect

Table 3. Details of Doppler lidar inter-comparison campaigns periods analysed in this work. A ray means one profile. Three rays per point means that data collected during three subsequent profile measurements to the specific measurement direction were taken into account to get one profile.

Time periods	Measurement setup	Tested parameter
The first inter-comparison period		
2–15 Sep 2011	<i>Lidars 32, 33, 34:</i> Focus at infinity Data integration: (a) vertical 150 000 pulses per ray (b) wind 150 000 pulses per ray, 3 rays per point	– Wind profiles every 10 min. – β profiles – β calibration
3 lidars side by side		
The second inter-comparison period		
20 Nov 2012 – 14 Dec 2012	<i>Lidar 34:</i> Focus at – 2 km (until 23 Nov 2012) – infinity (23 Nov 2012 onwards) Data integration: (a) vertical – 75 000 pulses per ray, 4 rays per point (until 23 Nov 2012) – 15 000 pulses per ray, 6 rays per point (23 Nov 2012 onwards) (b) wind – 75 000 pulses per ray, 4 rays per point (until 23 Nov 2012) – 15 000 pulses per ray, 4 rays per point (23 Nov 2012 onwards) (c) Custom scanning (a number of setups)	– Wind profiles every 3 min – β profiles – β calibration – Comparing different focus settings
3 lidars side by side, one lidar (no. 34) 100 m apart	<i>Lidar 46:</i> Focus at – 2 km (until 23 Nov 2012) – infinity (until 10 Dec 2012) – 1 km (10 Dec 2012 onwards) Data integration: (a) vertical 15 000 pulses per ray, 6 rays per point (b) wind 15 000 pulses per ray, 4 rays per point	
	<i>Lidar 53:</i> Focus at – 2 km until (23 Nov 2012) – infinity (23 Nov 2012 onwards) Data integration: (a) vertical 15 000 pulses per ray, 6 rays per point (b) wind 15 000 pulses per ray, 4 rays per point	
	<i>Lidar 54:</i> Focus at – 2 km (until 23 Nov 2012) – infinity (until 10 Dec 2012) – 2 km (10 Dec 2012 onwards) Data integration: (a) vertical 15 000 pulses per ray, 6 rays per point (b) wind 15 000 pulses per ray, 4 rays per point	
14 Dec 2012– 24 Jan 2013	<i>Lidar 34:</i> Focus at infinity Data integration: (a) vertical 15 000 pulses per ray, 6 rays per point (b) wind 15 000 pulses per ray, 4 rays per point (c) Custom scanning (a number of setups)	– Wind profiles every 3 min – β profiles – β calibration – Comparing different focus settings
2 lidars (no. 53, 54) side by side, lidar (no. 34) 100 m away	<i>Lidar 53:</i> Focus at infinity Data integration: (a) vertical 15 000 pulses per ray, 6 rays per point (b) wind 15 000 pulses per ray, 4 rays per point <i>Lidar 54:</i> Focus at 2 km Data integration: (a) vertical 15 000 pulses per ray, 6 rays per point (b) wind 15 000 pulses per ray, 4 rays per point	

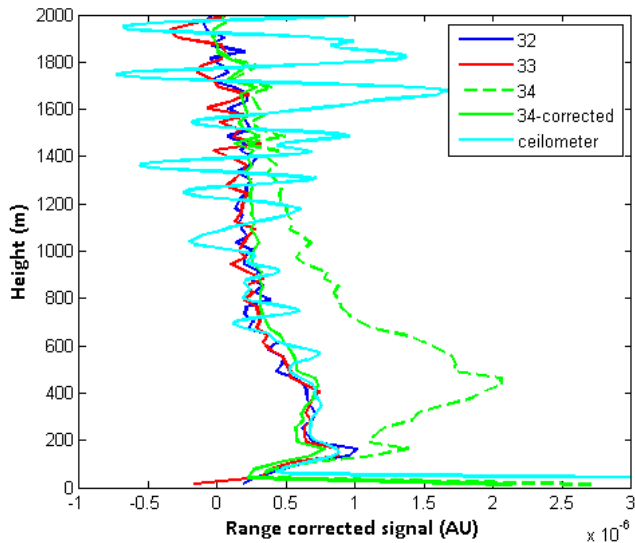


Fig. 5. Range-corrected signals from three Doppler lidars during the first inter-comparison campaign (04:18 UTC on 9 September 2011). An appropriately scaled co-located ceilometer profile is also shown. Doppler lidars 32 and 33 agree with each other and the less-sensitive ceilometer. Doppler lidar 34 clearly has an incorrect focus; after the new telescope focus is applied, together with a suitable calibration factor, it agrees with the other instruments.

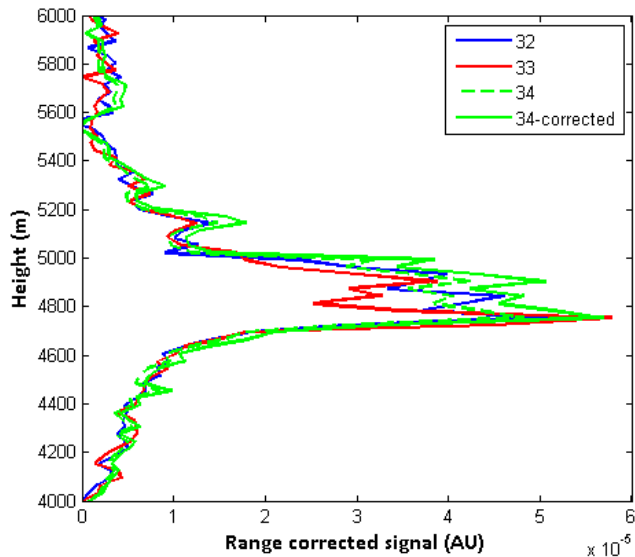


Fig. 6. As Fig. 5, except that the instrument range has been selected to encompass ranges at which cirrus may be present. Note that the co-located ceilometer was not sensitive enough to detect this particular cirrus cloud.

focus setting can also be identified by looking at returns from cirrus clouds (Fig. 6). This requires that at least one instrument has a known focus. Once the correct telescope focus and appropriate calibration factor is applied, the three instruments display similar attenuated backscatter profiles. The

Table 4. Statistical comparison of wind speed and wind direction measured with Doppler lidars. Shown are number of samples (N), root mean square error (RMSE), Pearson correlation (r) and slope of fitted linear curve (k). Data averaged over 15 min at range gates between 150 and 1050 m were included in the respective sample here. Episodes of snow, rain, cloud and wind direction change larger than 50° between subsequent profiles were excluded from the analysis here.

Lidar no.	N	k	R	RMSE
The first inter-comparison campaign: 2–15 Sep 2011				
34 vs. 32	8984			
speed		0.99	0.97	1.33
direction		0.99	0.99	10.31
34 vs. 33	8118			
speed		0.98	0.97	1.35
direction		0.99	0.99	10.94
32 vs. 33	8026			
speed		0.97	0.97	1.32
direction		1.00	0.99	10.72
The second inter-comparison campaign: 24 Nov–9 Dec 2012				
34 vs. 46	3435			
speed		0.90	0.93	1.55
direction		0.99	0.98	15.63
34 vs. 53	2977			
speed		0.87	0.90	1.87
direction		0.95	0.98	13.37
34 vs. 54	2846			
speed		0.87	0.91	1.81
direction		0.96	0.98	12.67
46 vs. 53	3461			
speed		0.92	0.91	1.72
direction		0.97	0.98	13.69
46 vs. 54	2977			
speed		0.91	0.92	1.62
direction		0.96	0.99	13.32
53 vs. 54	2622			
speed		0.92	0.93	1.48
direction		0.98	0.98	11.24

telescope function does not affect the Doppler velocity values, although an inadvertent erroneous focus may result in unexpected profiles of Doppler velocity uncertainties, since these depend on SNR.

Wind data were averaged over 15 min at each range gate and data from all available range gates between 150 and 1050 m are shown in Figs. 7 and 8, with the statistical results in Table 4. Data affected by clouds, rain or snow were excluded from the analysis. In addition, cases with highly varying wind direction ($> 50^\circ$) were excluded from analysis, since they introduced too much uncertainty in comparison

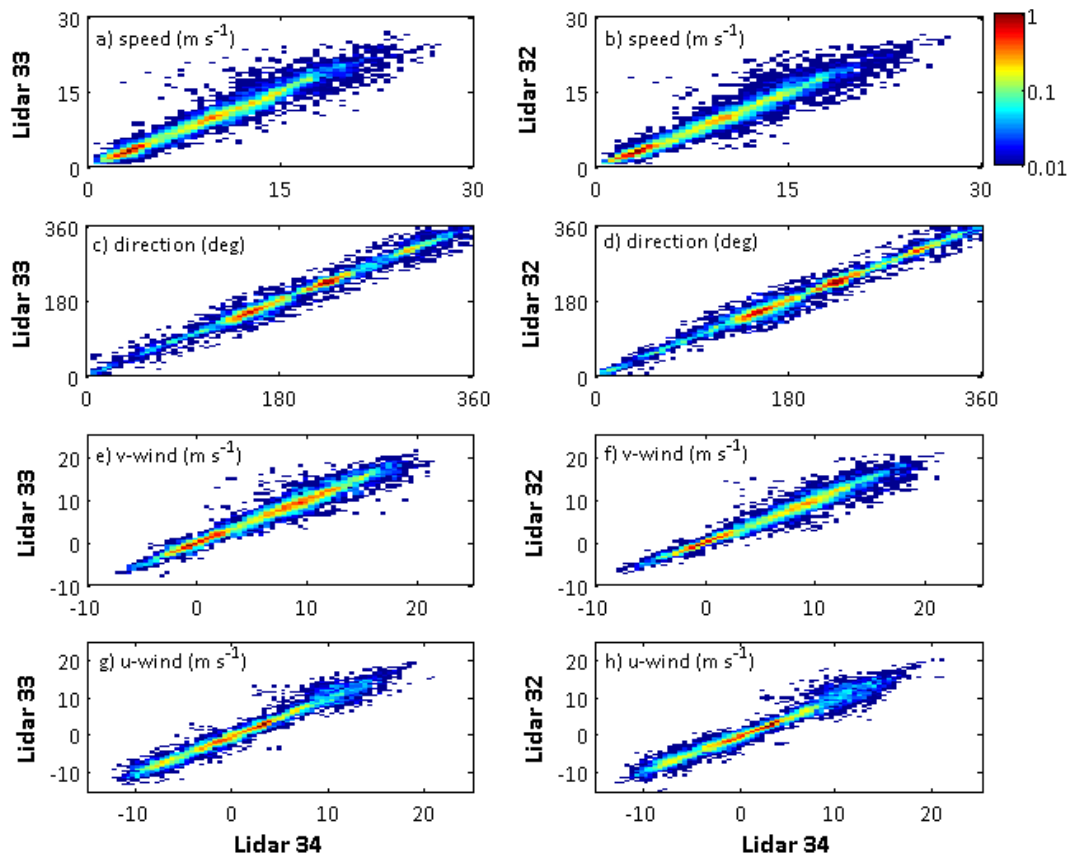


Fig. 7. Frequency of horizontal wind speed and direction, and v and u components of velocity measured during the first measurement campaign in Helsinki during the period 2–15 September 2011. Left panels show comparison of lidar 33 to lidar 34; right panels show comparison of lidars 32 and 34. Each point is an average over 15 min and all available data between 150 and 1050 m are shown. Pixel width for velocity and speed was 0.5 m s^{-1} , and for direction 5° .

that was independent from instrument operation. In Fig. 7 we analysed the measurement period 2–15 September 2011 and in Fig. 8 we analysed the period 24 November–9 December 2012. During these periods each lidar had similar settings of telescope focus length and data-averaging time (Table 3), except for Doppler lidar 34 during the first inter-comparison period.

Comparison of wind velocity u and v components, derived wind speed and direction showed generally good agreement between the instruments (Figs. 7 and 8, Table 4). The correlation coefficients were between 0.9 and 1 for wind speed and direction for each pair of lidars. Some deviation from the 1 : 1 line was evident and scattered points were observed. However, RMSE was always less than 2 m s^{-1} when wind speed was compared and less than 14° for directions.

Each wind profile is a snapshot. Therefore, each single wind profile represents a slightly different atmospheric situation. Thus, the statistical sampling is relatively poor due to the turbulent nature of the ABL within which these DBS measurements are obtained (Lane et al., 2013) and small deviations around the 1 : 1 line were expected. These results

also indicate that the observed differences in receiver sensitivity and telescope focus do not impact that much on the accuracy of wind observations, even though they affect the length of line of sight.

This was the first time that several identical Doppler lidars have been inter-compared to this level. Previously, vertical velocity and SNR profiles of two Streamline Doppler lidars have been inter-compared (Newson, 2012). Their results indicated reasonably good comparability of vertical velocity in regions with sufficient SNR. SNR profile figures showed small differences in SNR intensity.

4.2.3 Comparison of winds measured by Doppler lidar and sonic anemometers at SMEAR III and SMEAR IV

Comparisons were made between single range gate radial Doppler velocity and co-located sonic anemometer observations at SMEAR III in Helsinki. A profile of 2-D sonic anemometers (at 31, 35, 43, 59 m a.s.l.) was available from the SMEAR III station, about 60 m away from the Doppler lidar on the roof of FMI (44.4 m a.s.l.). Lidar data from

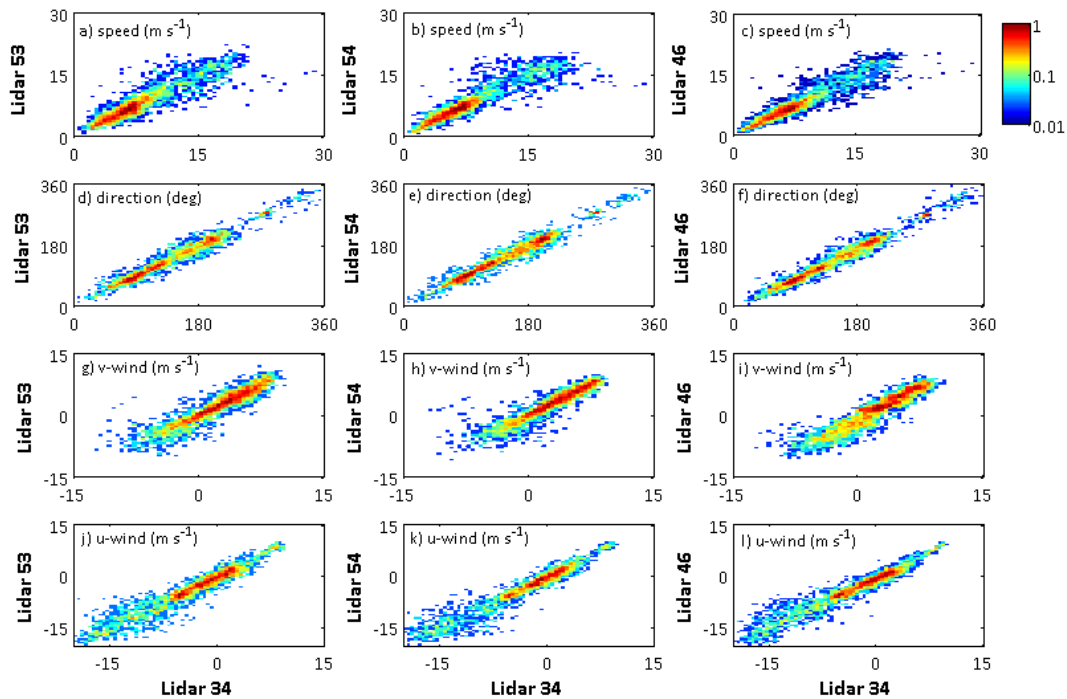


Fig. 8. Frequency of horizontal wind speed and direction, and v and u components of velocity measured during the second measurement campaign in Helsinki during the period 24 November–9 December 2012. Left panels show comparison of lidar 53 to lidar 34; middle panels compare lidar 54 versus 34; right panels compare lidars 46 and 34. Each point is an average over 15 min, and all available data between 150 and 1050 m are shown. Pixel width for velocity and speed was 0.5 m s^{-1} , and for direction 5° .

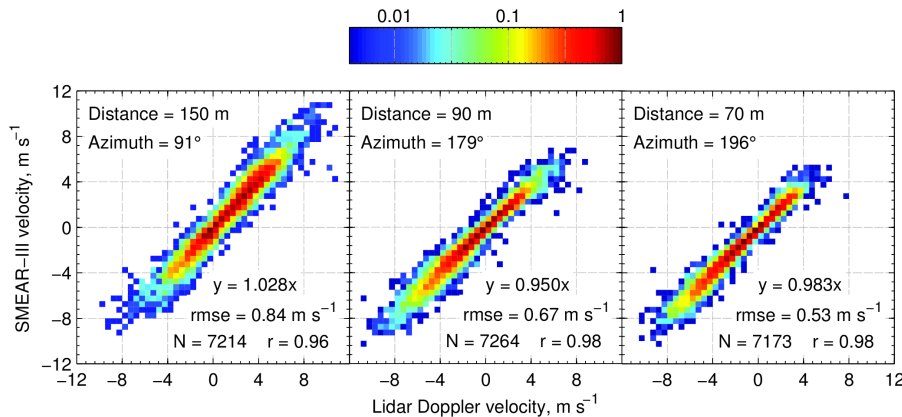


Fig. 9. Comparison of single-beam and range gate Doppler velocity with co-located sonic anemometer velocity: measurements with different horizontal separation from sonic anemometer are shown, and subsequent statistical parameters are also presented: number of half-an-hour mean velocity samples (N), root mean square error (RMSE), Pearson correlation (r) and slope of fitted linear curve.

three near-horizontal ($\sim 1^\circ$ elevation) beam directions (91° , 179° , 196°) were analysed. The horizontal difference between the centre of the first available lidar range gate (105 m) of the three beams and the anemometers was 150, 90 and 70 m, respectively. An average value of the two anemometers at 43 and 59 m best represents the chosen lidar range gate. Due to spatial differences in the related velocities we compare 30 min mean winds. Measurements took place

from 14 October 2011 to 20 June 2012. Sonic anemometer and Doppler lidar velocities show good comparability (Fig. 9, $r > 0.96$). The beam directions with a shorter horizontal separation to the anemometers have a better correspondence with the lidar. Perhaps surprisingly, the anemometer gives slightly lower wind values on average despite a slightly higher height. Overall, these observations are in accordance with similar lidar–sonic comparison measurements

performed with a Streamline Doppler lidar in London (Lane et al., 2013; Wood et al., 2013a).

Comparisons were made between single range gate (7th, i.e. 225 m above the lidar) Doppler lidar DBS wind speeds with sonic anemometer measurements at the Puijo tower at 220 m height above lake level during the period 20 September 2011–20 September 2012. Both sets of wind speeds were averaged over half an hour for the comparison. Due to the 2 km separation between the sensors, the correlation of all half-hourly averaged wind speeds was lower ($r=0.84$ for 17 494 all-weather cases, of which 5718 were fair-weather cases) than for the comparison at SMEAR IV. A closer correspondence has been observed previously for another type of Doppler lidar (Angelou et al., 2011). In addition, it seemed that in the presence of precipitation, correlation between the wind speed measurements (anemometer and Doppler lidar) decreased ($r=0.77$ for 4164 cases), which could be due to the increased uncertainty in Doppler lidar wind retrievals from falling targets in DBS volume. These observations show clearly that the separation distance is too large in this case for a definitive comparison. In future, sites at Vehmasmäki, Hyytiälä and Sodankylä offer the possibility for more comparisons with sonic anemometers mounted nearby in towers.

4.3 Towards scanning Doppler lidar operational applications

4.3.1 Effect of surface roughness on wind field

An advantage of the network is that at all our stations a clear line of sight of at least 90° in the azimuth direction, at elevations down to the lidar horizon, exists. Vertical azimuth display (VAD) and range height indicator (RHI) techniques are used, along with different combinations of custom-designed azimuth, elevation and temporal settings. In general our long-term aim is to develop new operational scanning strategies – and subsequent data-analysis methods – to be used for the characterization of ABL phenomena and meteorology, air-quality monitoring, cloud physics and weather forecasting. As an example, we have started 24-beam VAD wind scanning with the aim of improving the accuracy of wind profiles. In future, we may synchronize our wind measurement routines with other European sites. The paper by Banta et al. (2006) presents a technique to determine low-level nocturnal ABL heights from RHI scans. It is clear that other research disciplines such as wave or ice researchers (personal communications in FMI and UHEL) and the energy industry (Calpini et al., 2011) would also benefit from information on the temporal and spatial variation of surface wind field.

As an example we perform a VAD scan every 30 min at Utö. The VAD scan is taken at an elevation of 4° , with 24 beams (1 beam every 15° in azimuth and 5 s per beam). Near-horizontal scanning over the surface gives us primarily the Doppler velocity field (Fig. 10b). Using trigonometry we are able to estimate the spatially resolved horizontal wind

speed (U) and direction (φ) fields at each range gate based on radial Doppler velocity measurements (Wood et al., 2013a),

$$v_a = U \cdot \cos(\varphi - \theta_a), \quad (1)$$

$$v_b = U \cdot \cos(\varphi - \theta_b), \quad (2)$$

where v_a and v_b are Doppler velocity vectors of a pair of rays (a and b, respectively). U is wind speed and φ is the wind direction, which have to be assumed constant between the pair of rays; θ_a and θ_b are ray azimuths due north.

Due to the 4° beam elevation from the horizon, the range gate height from sea level increases with range from the lidar (at 1.5 km distance the range gate height is 104 m above the lidar horizon). When comparing corresponding range gates, and thus altitudes, we see from Fig. 10a and d how the wind speed and direction change perhaps due to the changing surface from sea to land, and how wind field changes between land and sea before and after an island by surrounded smaller islands on the north and east sides (not shown in Fig. 10a and d). In future, the analysis of long-term statistics of wind evolution over various surfaces will enable us to characterize the effect of these surfaces on air flow dynamics.

A simple confidence test for the method is to calculate the radial Doppler velocity using Eqs. (1) and (2). Only values of absolute velocity may be calculated because information on sign (i.e. direction) is lost when calculating wind speed and direction (Fig. 10e). When investigating differences between calculated and absolute values of measured radial velocity, it is clear that in the directions where wind speed and direction can be calculated from the main component of the velocity vector, we obtain best agreement (Fig. 10f). Results in directions of a minor velocity component can be used as indicative only. Nevertheless, these results indicate applicability of the method.

4.3.2 Air-quality monitoring with the Doppler lidars

In spring 2012, three Doppler lidars went operational (Table 1). On 22 May, two Doppler lidars observed increased depolarization ratio values in the non-cloudy ABL, indicative of a large fraction of nonspherical particles (e.g. fresh road dust or hydrophobic particles). Depolarization ratio profiles measured in Helsinki showed increased values throughout the ABL, while at Utö a new air mass with highly nonspherical particles advected over around 11:00 UTC (Fig. 11). However, at Utö the increased values were observed by in situ aerosol particle monitors for a short time only after 16:00 UTC. At Kuopio, the Doppler lidar showed moderate signals from moist ABL aerosol particles only in the co-channel.

Both ground-based and satellite-based aerosol optical depth (AOD; from MODIS_Terra and AQUA at 550 nm) observations showed increased values over southern Finland. In mid- and northern Finland, the AOD values were close to long-term averages. Further analysis of the aerosol particle dispersion in the ABL (i.e. Doppler lidar backscatter

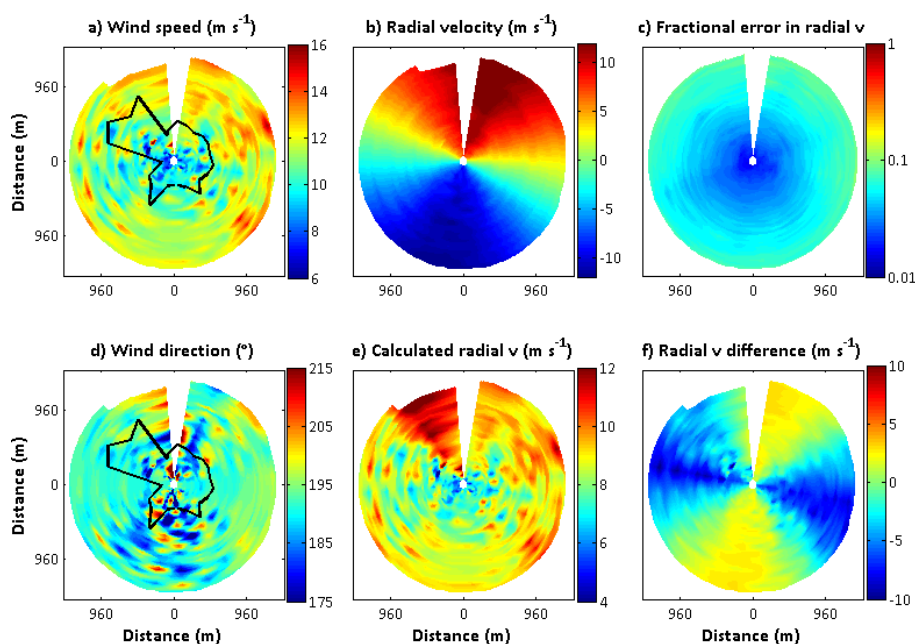


Fig. 10. Example of wind speed (a) and direction (d) near surface (with 4° elevation) using a Doppler-lidar scanning technique at Utö Island on 29 September 2012. The black curve is the border of Utö Island. A number of small islands on the northern and eastern side are not shown. Measured radial velocity (b) and its fractional error (c), calculated radial velocity (e) and difference of calculated and absolute value of measured radial velocity (f) are also shown.

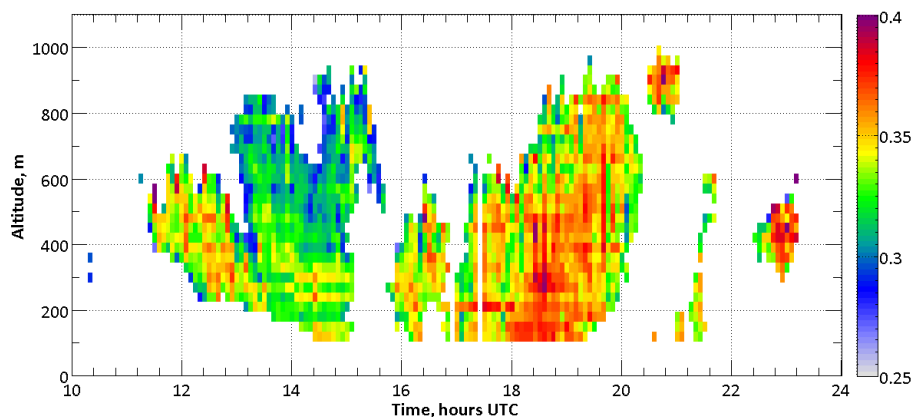


Fig. 11. Depolarization ratio profiles measured with the Doppler lidar at Utö on 22 May 2012.

and depolarization profiles), Doppler lidar vertical air motion, wind speed and direction profiles, and air-mass back-trajectories from the Air Resources Laboratory at the National Oceanic and Atmospheric Administration's Hybrid Single-Particle Lagrangian Integrated Trajectory (HYSPPLIT, version 4.8) model (Draxler and Hess, 2004; Air Resources Laboratory, 2011) indicated that, in southern continental Finland, increased depolarization values could be due to a mixture of road dust, which is a typical problem in spring time, and ash transported from forest fires near the Finnish southeastern border. However, a dust or ash episode from local sources at Utö would be unlikely to be responsible for the

observed aerosol particle depolarization ratio profiles. In addition, ground-based in situ data indicated a change in the aerosol particle population due to changing air mass, also seen in the Doppler lidar wind direction profiles, and the appearance of a new mode of 50–150 nm particles. Back-trajectory analysis confirmed that air masses came via southern Finland and forest fire areas in western Russia.

This example has demonstrated that, by combining observations of the Doppler lidar network and in situ sensors, we get more comprehensive information on ABL aerosol and air quality. However, air mass back-trajectories provide important ancillary information. The lidar depolarization ratio

method is limited to nonspherical or nearly nonspherical targets due to the low SNR in Finland, and thus pollution of hydrophilic particles or particles suspended long enough in the moist ABL are not detected in the cross-channel. This may be improved by developing data analysis methods to deploy raw data instead of measurement software pre-processed data, which is currently used in our data analysis.

5 Concluding remarks

A new ground-based remote sensing network has been established in Finland. The main objectives of the remote-sensing network are to provide information on aerosol particles, wind, ABL evolution, clouds, precipitation and related processes for now-casting, air quality, the public, the aviation safety authority and climate prediction. Different to other similar nationwide infrastructures, Finland's remote-sensing network allows research in a variety of environments: (i) from urban to rural to marine environments, and (ii) from continental to Arctic climates. Instrumentation consists of passive (e.g. sunphotometers, microwave radiometers) and active (e.g. Doppler lidars, cloud radar, Raman lidar, ceilometers) remote sensors. In addition, extensive possibilities for synergy of in situ and remote-sensing sensors, and co-operation across research disciplines are advantages to the Finnish remote-sensing infrastructure.

There is a Doppler lidar at each station. Therefore, performance of the Doppler lidars was investigated during two inter-comparison campaigns in Helsinki. Our scope was to investigate comparability of backscattered signal and wind, which is important since these devices are already placed at different sites across Finland. The results indicated good comparability of investigated wind quantities between Doppler lidars and reference in situ wind observations. In the beginning, SNR profiles showed disagreement between the lidars which arose from the inaccurate telescope focus setting of one of the lidars and different calibrations. However, after using telescope focus length corresponding overlap functions and taking into account calibration, SNR profiles showed similar shape between the lidars. In addition, Doppler lidar aerosol profiling (i.e. attenuated backscatter coefficient and depolarization ratio) performance should be compared with the Polly^{XT}. When knowing these differences, we are able to consider them in data analysis and subsequent conclusions. In addition, Doppler lidar operational reliability and capability was investigated. Harsh winters, and low ambient aerosol particle load, limits data coverage. Thus, care must be taken on maintenance during winter and novel data analysis methods need to be developed.

In the future, we expect to continuously extend our ground-based remote-sensing network and improve its capability by developing data-processing methods. One of our plans is to increase backscatter profile collection from the existing ceilometer network. In 2014, a project "Biogenic

Aerosols: Effects on Clouds and Climate (BEACC)" began at Hyytiälä. The project hosts a comprehensive ground-based remote-sensing facility, the ARM Climate Research Facility. Additionally, full capability of the current instrumentation will be deployed.

Supplementary material related to this article is available online at <http://www.atmos-meas-tech.net/7/1351/2014/amt-7-1351-2014-supplement.pdf>.

Acknowledgements. The research leading to these results has received funding from the European Union Seventh Framework Programme (FP7/2007-2013) under grant agreement no. 262254 (ACTRIS), the Academy of Finland, Centre of Excellence Programme (project 1118615) and the Academy of Finland FIRI-funding "Infrastructure of Environmental and Atmospheric Sciences" (ATM-Science, project 141451). Curtis Wood acknowledges funding from EC FP7 ERC Grant 227915 (Atmospheric planetary boundary layers – physics, modelling and role in 6 Earth system). People maintaining the SMEAR, Utö and Sodankylä stations are acknowledged.

The service charges for this open access publication have been covered by a Research Centre of the Helmholtz Association.

Edited by: V. Amiridis

References

- Aaltonen, V., Rodriguez, E., Kazadzis, S., Arola, A., Amiridis, V., Lihavainen, H., and de Leeuw, G.: On the variation of aerosol properties over Finland based on the optical columnar measurements, *Atmos. Res.*, 116, 46–55, doi:10.1016/j.atmosres.2011.07.014, 2012.
- Aarnio, P., Yli-Tuomi, T., Kousa, A., Mäkelä, T., Hirsikko, A., Hämeri, K., Räisänen, M., Hillamo, R., Koskentalo, T., and Jantunen, M.: The concentrations and composition of and exposure to fine particles (PM_{2.5}) in the Helsinki subway system, *Atmos. Environ.*, 39, 5059–5066, 2005.
- ACIA – Arctic climate impact assessment: Cambridge University Press, New York, USA, 2005.
- Air Resources Laboratory: Gridded Meteorological Data Archives, available at: <http://www.arl.noaa.gov/archives.php> (last access: 31 August 2012), 2011.
- Albrecht, B. A.: Aerosols, cloud microphysics, and fractional cloudiness, *Science*, 245, 1227–1230, 1989.
- Althausen, D., Engelmann, R., Baars, H., Heese, B., Ansmann, A., Müller, D., and Komppula, M.: Portable Raman Lidar Polly^{XT} for Automated Profiling of Aerosol Backscatter, Extinction, and Depolarization, *J. Atmos. Ocean. Tech.*, 26, 2366–2378, doi:10.1175/2009JTECHA1304.1, 2009.
- Ansmann, A., Riebesell, M., Wandinger, U., Weitkamp, C., Voss, E., Lahmann, W., and Michaelis, W.: Combined Raman Elastic-Backscatter LIDAR for Vertical Profiling of Moisture, Aerosol Extinction, Backscatter, and LIDAR Ratio, *Appl. Phys. B*, 55, 18–28, 1992.

- Angelou, N., Bingöl, F., Courtney, M., Diznabi, B., Foussekis, D., Gottschall, D., Hansen, K. H., Jørgensen, H. E., Kristensen, L., Larsen, G. C., Lindelöw-Marsden, P., Mann, J., Mikkelsen, T., Paulsen, U. S., Pedersen, T. F., Peña, A., Sathe, A., Sjöholm, M., and Wagner, R.: Advancements in Wind Energy Metrology UP-WIND 1A2.3, in: *Risø-R-1752(EN)*, edited by: Pedersen, T. F. and Wagner, R., Technical University Denmark, Risø National laboratory for Sustainable Energy, Risø, Denmark, 2011.
- Ansmann, A., Tesche, M., Seifer, P., Gross, S., Freudenthaler, V., Apituley, A., Wilson, K. M., Serikov, I., Linné, H., Heinold, B., Hiebsch, A., Schnell, F., Schmidt, J., Mattis, I., Wandinger, U., and Wiegner, M.: Ash and fine-mode particle mass profiles from EARLINET-AERONET observations over central Europe after the eruptions of the Eyjafjallajökull volcano in 2010, *J. Geophys. Res.*, 116, D00U02, doi:10.1029/2010JD015567, 2011.
- Banta, R. M., Pichugina, Y. L., and Brewer, W. A.: Turbulent velocity-variance profiles in the stable boundary layer generated by a nocturnal low-level jet, *J. Atmos. Sci.*, 63, 2700–2719, 2006.
- Barlow, J. F. and Coceal, O.: A review of urban roughness sublayer turbulence, Tech. Rep., Met Office, Exeter, p. 68, 2009.
- Barlow, J. F., Dunbar, T. M., Nemitz, E. G., Wood, C. R., Gallagher, M. W., Davies, F., O'Connor, E., and Harrison, R. M.: Boundary layer dynamics over London, UK, as observed using Doppler lidar during REPARTEE-II, *Atmos. Chem. Phys.*, 11, 2111–2125, doi:10.5194/acp-11-2111-2011, 2011.
- Bony, S., Colman, R., Kattsov, V. M., Allan, R. P., Bretherton, C. S., Dufresne, J.-L., Hall, A., Hallegatte, S., Holland, M. M., Ingram, W., Randall, D. A., Soden, B. J., Tselioudis, G., and Webb, M. J.: How Well Do We Understand and Evaluate Climate Change Feedback Processes?, *J. Climate*, 19, 3445–3482, 2006.
- Bösenberg, J., Matthias, J., Amodeo, A., Amoiridis, V., Ansmann, A., Baldasano, J. M., Balin, I., Balis, D., Böckmann, C., Boselli, A., Carlsson, G., Chaikovskiy, A., Chourdakis, G., Comerón, A., De Tomasi, F., Eixmann, R., Freudenthaler, V., Giehl, H., Grigorov, I., Hågård, A., Iarlori, M., Kirsche, A., Kolarov, G., Komguem, L., Kreipl, S., Kumpf, W., Larchevêque, G., Linné, H., Matthey, R., Mattis, I., Mekler, A., Mironova, I., Mitev, V., Mona, L., Müller, D., Music, S., Nickovic, S., Pandolfi, M., Pappayannis, A., Pappalardo, G., Pelon, J., Pérez, C., Perrone, R. M., Persson, R., Resendes, D. P., Rizi, V., Rocadenbosch, F., Rodrigues, J. A., Sauvage, L., Schneidenbach, L., Schumacher, R., Shcherbakov, V., Simeonov, V., Sobolewski, P., Spinelli, N., Stachlewska, I., Stoyanov, D., Trickl, T., Tsaknakis, G., Vaughan, G., Wandinger, U., Wang, X., Wiegner, M., Zavrtnik, M., and Zerefos, C.: EARLINET: A European Aerosol Research Lidar Network to Establish an Aerosol Climatology, Report no. 348, Max Planck Institute for Meteorology, Hamburg, 2003.
- Calpini, B., Ruffieux, D., Bettems, J.-M., Hug, C., Huguenin, P., Isaak, H.-P., Kaufmann, P., Maier, O., and Steiner, P.: Ground-based remote sensing profiling and numerical weather prediction model to manage nuclear power plants meteorological surveillance in Switzerland, *Atmos. Meas. Tech.*, 4, 1617–1625, doi:10.5194/amt-4-1617-2011, 2011.
- Chen, Y. and Penner, J. E.: Uncertainty analysis for estimates of the first indirect aerosol effect, *Atmos. Chem. Phys.*, 5, 2935–2948, doi:10.5194/acp-5-2935-2005, 2005.
- Chiu, J. C., Huang, H.-C., Marshak, A., Slutsker, I., Giles, D. M., Holben, B. N., Knyazikhin, Y., and Wiscombe, W. J.: Cloud optical depth retrievals from the Aerosol Robotic Network (AERONET), *J. Geophys. Res.*, 115, D14202, doi:10.1029/2009JD013121, 2010.
- Cimini, D., Hewison, T. J., Martin, L., Güldner, J., Gaffard, C., and Marzano, F. S.: Temperature and humidity profile retrievals from ground-based microwave radiometers during TUC, *Meteorol. Z.*, 15, 45–56, 2006.
- Collier, C. G., Davies, F., and Pearson, G. N.: The land below the wind: Doppler LIDAR observations from the tropical rain forest of Sabah, Borneo, Malaysia, *R. Met. S. Weather*, 65, 45–50, 2010.
- Dal Maso, M., Hyvärinen, A., Komppula, M., Tunved, P., Kerminen, V.-M., Lihavainen, H., Viisanen, Y., Hansson, H.-C., and Kulmala, M.: Annual and interannual variation in boreal forest aerosol particle number and volume concentration and their connection to particle formation, *Tellus B*, 60, 495–508, 2008.
- Delanoë, J., Hogan, R. J., Forbes, R. M., Bodas-Salcedo, A., and Stein, T. H. M.: Evaluation of ice cloud representation in the ECMWF and UK Met Office models using CloudSat and CALIPSO data, *Q. J. Roy. Meteorol. Soc.*, 137, 2064–2078, 2011.
- Draxler, R. R. and Hess, G. D.: Description of the HYSPLIT 4 Modelling System, NOAA Technical Memorandum ERL ARL-224, Air Resources Laboratory, Silver Spring, Maryland, 2004.
- Emeis, S., Schäfer, K., and Munkel, C.: Surface-based remote sensing of the mixing-layer height — a review, *Meteorol. Z.*, 17, 621–630, 2008.
- Engelmann, R., Wandinger, U., Ansmann, A., Müller, D., Žeromskis, E., Althausen, D., and Wehner, B.: Lidar Observations of the Vertical Aerosol Flux in the Planetary Boundary Layer, *J. Atmos. Ocean. Tech.*, 25, 1296–1306, 2008.
- Engelmann, R., Althausen, D., Heese, B., Baars, H., and Komppula, M.: Recent upgrades of the multiwavelength polarization Raman lidar Polly^{XT}, Proceedings of the International Laser Radar Conference, Porto Heli, Greece, 2012.
- Engler, C., Lihavainen, H., Komppula, M., Kerminen, V.-M., and Kulmala, M.: Continuous measurements of aerosol properties at the Baltic Sea, *Tellus B*, 59, 728–741, 2007.
- Flentje, H., Heese, B., Reichardt, J., and Thomas, W.: Aerosol profiling using the ceilometer network of the German Meteorological Service, *Atmos. Meas. Tech. Discuss.*, 3, 3643–3673, doi:10.5194/amtd-3-3643-2010, 2010.
- Freudenthaler, V., Esselborn, M., Wiegner, M., Heese, B., Tesche, M., Ansmann, A., Müller, D., Althausen, D., Wirth, M., Fix, A., Ehret, G., Knippertz, P., Toledano, C., Gasteiger, J., Garhammer, M., and Seefeldner, M.: Depolarization ratio profiling at several wavelengths in pure Saharan dust during SAMUM 2006, *Tellus B*, 61, 165–179, doi:10.1111/j.1600-0889.2008.00396.x, 2009.
- Ghamberg, M., Savijärvi, H., and Leskinen, M.: The influence of synoptic scale flow on sea breeze induced surface winds and calm zones, *Tellus A*, 62, 209–217, 2010.
- Görsdorf, U., Seifert, A., Lehmann, V., and Köhler, M.: Cloud statistics and NWP-model validation based on long-term measurements of a 35 GHz radar, Proceedings of 35th Conference on Radar Meteorology, Pittsburgh, PA, USA, 2011.

- Haefelin, M., Angelini, F., Morille, Y., Martucci, G., Frey, S., Gobbi, G. P., Lolli, S., O'Dowd, C. D., Sauvage, L., Xueref-Rémy, L., Wastine, B., and Feist, D. G.: Evaluation, of mixing-height retrievals from automatic profiling lidars and ceilometers in view of future integrated networks in Europe, *Bound.-Lay. Meteorol.*, 143, 49–75, 2012.
- Hari, P. and Kulmala, M.: Station for Measuring Ecosystem-Atmosphere Relations (SMEAR II), *Boreal Environ. Res.*, 10, 315–322, 2005.
- Harvey, N. J., Hogan, R. J. and Dacre, H. F.: A method to diagnose boundary-layer type using Doppler lidar, *Q. J. Roy. Meteorol. Soc.*, 139, 1681–1693, doi:10.1002/qj.2068, 2013.
- Hegg, D. A., Covert, D. S., Jonsson, H. H., and Woods, R. K.: A simple relationship between cloud drop number concentration and precursor aerosol concentration for the regions of Earth's large marine stratocumulus decks, *Atmos. Chem. Phys.*, 12, 1229–1238, doi:10.5194/acp-12-1229-2012, 2012.
- Henderson, S. W., Gatt, P., Rees, D., and Huffaker, R. M.: Wind Lidar, in *Laser Remote Sensing*, Eds. Fujii and Fukuchi, CRC Press, Taylor and Francis Group, Boca Raton, FL, 469–722, 2005.
- Heymsfield, A. J., Bansemer, A., Field, P. R., Durden, S. L., Stith, J. L., Dye, J. E., Hall, W., and Grainger, C. A.: Observations and Parametrizations of Particle Size Distributions in Deep Tropical Cirrus and Stratiform Precipitating Clouds: Results from In Situ Observations in TRMM Field Campaigns, *J. Atmos. Sci.*, 59, 3457–3491, 2002.
- Heywood, J. and Boucher, O.: Estimates of the direct and indirect radiative forcing due to tropospheric aerosols: a review, *Rev. Geophys.*, 38, 513–543, 2000.
- Hirsikko, A., Vakkari, V., Tiitta, P., Hatakka, J., Kerminen, V.-M., Sundström, A.-M., Beukes, J. P., Manninen, H. E., Kulmala, M., and Laakso, L.: Multiple daytime nucleation events in semi-clean savannah and industrial environments in South Africa: analysis based on observations, *Atmos. Chem. Phys.*, 13, 5523–5532, doi:10.5194/acp-13-5523-2013, 2013.
- Hogan, R. J., Mittermaier, M. P., and Illingworth, A. J.: The retrieval of ice water from radar reflectivity factor and temperature and its use in the evaluation of a mesoscale model, *J. Appl. Meteorol. Clim.*, 45, 301–317, 2006.
- Hogan, R. J., Grant, A. L. M., Illingworth, A. J., Pearson, G. N., and O'Connor, E. J.: Vertical velocity variance and skewness in clear and cloud-topped boundary layers as revealed by Doppler lidar, *Q. J. Roy. Meteorol. Soc.*, 135, 635–643, 2009.
- Holben, B. N., Eck, T. F., Slutsker, I., Tanré, D., Buisk, J. P., Setzer, A., Vermote, E., Reagan, J. A., Kaufman, Y. J., Nakajima, T., Lavenu, F., Jankowiak, I., and Smirnov, A.: AERONET – A Federated Instrument Network and Data Archive for Aerosol Characterization, *Remote Sens. Environ.*, 66, 1–16, 1998.
- Hou, A. Y., Skofronick-Jackson, G., Kummerow, C. D., and Shepherd, J. M.: Global precipitation measurements, in: *Precipitation: Advances in Measurement, Estimation and Prediction*, edited by: Michaelides, S., Springer-Verlag, Berlin, Heidelberg, 2008.
- Hussein, T., Kukkonen, J., Korhonen, H., Pohjola, M., Pirjola, L., Wraith, D., Härkönen, J., Teinilä, K., Koponen, I. K., Karppinen, A., Hillamo, R., and Kulmala, M.: Evaluation and modeling of the size fractionated aerosol particle number concentration measurements nearby a major road in Helsinki – Part II: Aerosol measurements within the SAPHIRE project, *Atmos. Chem. Phys.*, 7, 4081–4094, doi:10.5194/acp-7-4081-2007, 2007.
- Hyvärinen, A.-P., Komppula, M., Engler, C., Kivekäs, N., Kerminen, V.-M., Dal Maso, M., Viisanen, Y., and Lihavainen, H.: Atmospheric new particle formation at Utö, Baltic Sea 2003–2005, *Tellus B*, 60, 345–352, 2008.
- Illingworth, A. J., Hogan, R. J., O'Connor, E. J., Bouniol, D., Brooks, M. E., Delanoë, J., Donovan, D. P., Eastment, J. D., Gaussiat, N., Goddard, J. W. F., Haefelin, M., Klein baltink, H., Krasnov, O. A., Pelon, J., Piriou, J.-M., Protat, A., Russchenberg, H. W. J., Seifert, A., Tompkins, A. M., van Zadelhoff, G.-J., Vinit, F., Willén, U., Wilson, D. R., and Wrench, C. L.: CLOUDNET: Continuous Evaluation of Cloud Profiles in Seven Operational Models Using Ground-Based Observations, *B. Am. Meteorol. Soc.*, 88, 883–898, doi:10.1175/BAMS-88-6-883, 2007.
- Iivesniemi, H., Levula, J., Ojansuu, R., Kolari, P., Kulmala, L., Pumpanen, J., Launiainen, S., Vesala, T., and Nikinmaa, E.: Long-term measurements of the carbon balance of a boreal Scots pine dominated forest ecosystem, *Boreal Environ. Res.*, 14, 731–753, 2009.
- Iivesniemi, H., Pumpanen, J., Duursma, R., Hari, P., Keronen, P., Kolari, P., Kulmala, M., Mammarella, I., Nikinmaa, E., Rannik, Ü., Pohja, T., Siivola, E., and Vesala, T.: Water balance of a boreal Scots pine forest, *Boreal Environ. Res.*, 15, 375–396, 2010.
- Immler, F., Treffeisen, R., Engelbart, D., Krüger, K., and Schrems, O.: Cirrus, contrails, and ice supersaturated regions in high pressure systems at northern mid latitudes, *Atmos. Chem. Phys.*, 8, 1689–1699, doi:10.5194/acp-8-1689-2008, 2008.
- IPCC: Climate Change 2007: The Physical Science Basis, in: *Contribution of Working Group I to the Fourth Assessment Report of the Intergovernmental Panel on Climate Change*, edited by: Solomon, S., Qin, D., Manning, M., Chen, Z., Marquis, M., Averyt, K. B., Tignor, M., and Miller, H. L., Cambridge University Press, Cambridge, UK and New York, NY, USA, 996 pp., 2007.
- Janssen, R. H. H., Vilà-Guerau de Arellano, J., Ganzeveld, L. N., Kabat, P., Jimenez, J. L., Farmer, D. K., van Heerwaarden, C. C., and Mammarella, I.: Combined effects of surface conditions, boundary layer dynamics and chemistry on diurnal SOA evolution, *Atmos. Chem. Phys.*, 12, 6827–6843, doi:10.5194/acp-12-6827-2012, 2012.
- Järvi, L., Hannuniemi, H., Hussein, T., Junninen, H., Aalto, P. P., Hillamo, R., Mäkelä, T., Keronen, P., Siivola, E., Vesala, T., and Kulmala, M.: The urban measurement station SMEAR III: Continuous monitoring of air pollution and surface-atmosphere interactions in Helsinki, Finland, *Boreal Environ. Res.*, 14, 86–109, 2009a.
- Järvi, L., Rannik, Ü., Mammarella, I., Sogachev, A., Aalto, P. P., Keronen, P., Siivola, E., Kulmala, M., and Vesala, T.: Annual particle flux observations over a heterogeneous urban area, *Atmos. Chem. Phys.*, 9, 7847–7856, doi:10.5194/acp-9-7847-2009, 2009b.
- Järvi, L., Nordbo, A., Junninen, H., Riikonen, A., Moilanen, J., Nikinmaa, E., and Vesala, T.: Seasonal and annual variation of carbon dioxide surface fluxes in Helsinki, Finland, in 2006–2010, *Atmos. Chem. Phys.*, 12, 8475–8489, doi:10.5194/acp-12-8475-2012, 2012.

- Juga, I., Hippi, M., Moisseev, D., and Saltikoff, E.: Analysis of weather factors responsible for the traffic 'Black Day' in Helsinki, Finland, on 17 March 2005, *Meteorol. Appl.*, 19, 1–9, 2012.
- Kamphus, M., Ettner-Mahl, M., Klimach, T., Drewnick, F., Keller, L., Cziczko, D. J., Mertes, S., Borrmann, S., and Curtius, J.: Chemical composition of ambient aerosol, ice residues and cloud droplet residues in mixed-phase clouds: single particle analysis during the Cloud and Aerosol Characterization Experiment (CLACE 6), *Atmos. Chem. Phys.*, 10, 8077–8095, doi:10.5194/acp-10-8077-2010, 2010.
- Kivi, R., Kyrö, E., Turunen, T., Ulich, T., and Turunen, E.: Atmospheric Trends above Finland: II Troposphere and Stratosphere, *Geophysica*, 35, 71–85, 1999.
- Kolmonen, P., Sundström, A.-M., Sogacheva, L., Rodriguez, E., Virtanen, T., and de Leeuw, G.: Uncertainty characterization of AOD for the AATSR dual and single view retrieval algorithms, *Atmos. Meas. Tech. Discuss.*, 6, 4039–4075, doi:10.5194/amtd-6-4039-2013, 2013.
- Komppula, M., Mielonen, T., Arola, A., Korhonen, K., Lihavainen, H., Hyvärinen, A.-P., Baars, H., Engelmann, R., Althausen, D., Ansmann, A., Müller, D., Panwar, T. S., Hooda, R. K., Sharma, V. P., Kerminen, V.-M., Lehtinen, K. E. J., and Viisanen, Y.: Technical Note: One year of Raman-lidar measurements in Gual Pahari EUCAARI site close to New Delhi in India – Seasonal characteristics of the aerosol vertical structure, *Atmos. Chem. Phys.*, 12, 4513–4524, doi:10.5194/acp-12-4513-2012, 2012.
- Korhonen, K., Giannakaki, E., Mielonen, T., Pfüller, A., Laakso, L., Vakkari, V., Baars, H., Engelmann, R., Beukes, J. P., Van Zyl, P. G., Ramandh, A., Ntsangwane, L., Josipovic, M., Tiitta, P., Fourie, G., Ngwana, I., Chiloane, K., and Komppula, M.: Atmospheric boundary layer top height in South Africa: measurements with lidar and radiosonde compared to three atmospheric models, *Atmos. Chem. Phys.*, 14, 4263–4278, doi:10.5194/acp-14-4263-2014, 2014.
- Koskinen, J. T., Poutiainen, J., Schultz, D. M., Joffe, S., Koistinen, J., Saltikoff, E., Gregow, E., Turtiainen, H., Dabberdt, W. F., Damski, J., Eresmaa, N., Göke, S., Hyvärinen, O., Järvi, L., Karppinen, A., Kotro, J., Kuitunen, T., Kukkonen, J., Kulmala, M., Moisseev, D., Nurmi, P., Pohjola, H., Pylkkö, P., Vesala, T., and Viisanen, Y.: The Helsinki TESTBED, *B. Am. Meteorol. Soc.*, 92, 325–342, doi:10.1175/2010BAMS2878.1, 2011.
- Kulmala, M. and Tammet, H.: Finnish-Estonian air ion and aerosol workshops, *Boreal Environ. Res.*, 12, 237–245, 2007.
- Kulmala, M., Hämeri, K., Aalto, P. P., Mäkelä, J. M., Pirjola, L., Nilsson, E. D., Buzorius, G., Rannik, Ü., Dal Maso, M., Seidl, W., Hoffman, T., Janson, R., Hansson, H.-C., Viisanen, Y., Laaksonen, A., and O'Dowd, C. D.: Overview of the international project on biogenic aerosol formation in the boreal forest (BIOFOR), *Tellus B*, 53, 324–343, 2001.
- Laitinen, T., Ehn, M., Junninen, H., Ruiz-Jimenez, J., Prshintsev, J., Hartonen, K., Riekkola, M.-L., Worsnop, D. R., and Kulmala, M.: Characterization of organic compounds in 10- to 50-nm aerosol particles in boreal forest with laser desorption-ionization aerosol mass spectrometer and comparison with other techniques, *Atmos. Environ.*, 45, 3711–3719, 2011.
- Lane, S. E., Barlow, J. F., and Wood, C. R.: An assessment of a three-beam Doppler lidar wind profiling method for use in urban areas, *J. Wind Eng. Ind. Aerod.*, 119, 53–59, 2013.
- Launiainen, S.: Seasonal and inter-annual variability of energy exchange above a boreal Scots pine forest, *Biogeosciences*, 7, 3921–3940, doi:10.5194/bg-7-3921-2010, 2010.
- Leskinen, A., Portin, H., Komppula, M., Miettinen, P., Arola, A., Lihavainen, H., Hatakka, J., Laaksonen, A., and Lehtinen, K. E. J.: Overview of the research activities and results at Puijo semi-urban measurement station, *Boreal Environ. Res.*, 14, 576–590, 2009.
- Leskinen, A., Arola, A., Komppula, M., Portin, H., Tiitta, P., Miettinen, P., Romakkaniemi, S., Laaksonen, A., and Lehtinen, K. E. J.: Seasonal cycle and source analyses of aerosol optical properties in a semi-urban environment at Puijo station in Eastern Finland, *Atmos. Chem. Phys.*, 12, 5647–5659, doi:10.5194/acp-12-5647-2012, 2012.
- Leskinen, M., Markkula, I., Koistinen, J., Pylkkö, P., Ooperi, S., Siljamo, P., Ojanen, H., Raiskio, S., and Tiilikkala, K.: Pest insect immigration warning by an atmospheric dispersion model, weather radars and traps, *J. Appl. Entomol.*, 135, 55–67, 2011.
- Lihavainen, H., Kerminen, V.-M., and Remer, L. A.: Aerosol-cloud interaction determined by both in situ and satellite data over a northern high-latitude site, *Atmos. Chem. Phys.*, 10, 10987–10995, doi:10.5194/acp-10-10987-2010, 2010.
- Lohmann, U. and Feichter, J.: Global indirect aerosol effects: a review, *Atmos. Chem. Phys.*, 5, 715–737, doi:10.5194/acp-5-715-2005, 2005.
- Lohmann, U., Rotstajn, L., Storelvmo, T., Jones, A., Menon, S., Quaas, J., Ekman, A. M. L., Koch, D., and Ruedy, R.: Total aerosol effect: radiative forcing or radiative flux perturbation?, *Atmos. Chem. Phys.*, 10, 3235–3246, doi:10.5194/acp-10-3235-2010, 2010.
- Madonna, F., Amodeo, A., Boselli, A., Cornacchia, C., Cuomo, V., D'Amico, G., Giunta, A., Mona, L., and Pappalardo, G.: CIAO: the CNR-IMAA advanced observatory for atmospheric research, *Atmos. Meas. Tech.*, 4, 1191–1208, doi:10.5194/amt-4-1191-2011, 2011.
- Makkonen, R., Asmi, A., Kerminen, V.-M., Boy, M., Arneth, A., Hari, P., and Kulmala, M.: Air pollution control and decreasing new particle formation lead to strong climate warming, *Atmos. Chem. Phys.*, 12, 1515–1524, doi:10.5194/acp-12-1515-2012, 2012.
- Manninen, H. E., Petäjä, T., Asmi, E., Riipinen, I., Nieminen, T., Mikkilä, J., Hörrak, U., Mirme, A., Mirme, S., Laakso, L., Kerminen, V.-M., and Kulmala, V.-M.: Long-term field measurements of charged and neutral clusters using Neutral cluster and Air Ion Spectrometer (NAIS), *Boreal Environ. Res.*, 14, 591–605, 2009.
- Marinoni, A., Laj, P., Sellegri, K., and Mailhot, G.: Cloud chemistry at the Puy de Dôme: variability and relationships with environmental factors, *Atmos. Chem. Phys.*, 4, 715–728, doi:10.5194/acp-4-715-2004, 2004.
- McFiggans, G., Artaxo, P., Baltensperger, U., Coe, H., Facchini, M. C., Feingold, G., Fuzzi, S., Gysel, M., Laaksonen, A., Lohmann, U., Mentel, T. F., Murphy, D. M., O'Dowd, C. D., Snider, J. R., and Weingartner, E.: The effect of physical and chemical aerosol properties on warm cloud droplet activation, *Atmos. Chem. Phys.*, 6, 2593–2649, doi:10.5194/acp-6-2593-2006, 2006.
- McLaughlin, D. J., Knapp, E. A., Wang, Y., and Chandrasekar, V.: Distributed weather radar using X-band active arrays, *IEEE Aerospace Elect. Syst. Mag.*, 7, 21–26, 2009.

- Milroy, C., Martucci, G., Lolli, S., Loaec, S., Sauvage, L., Xueref-Remy, I., Lavric, J. V., Ciais, P., and O'Dowd, C. D.: On the ability of pseudo-operational ground-based light detection and ranging (LIDAR) sensors to determine boundary-layer structure: intercomparison and comparison with in-situ radiosounding, *Atmos. Meas. Tech. Discuss.*, 4, 563–597, doi:10.5194/amtd-4-563-2011, 2011.
- Müller, D., Wandinger, U., and Ansmann, A.: Microphysical particle parameters from extinction and backscatter lidar data by inversion with regularization: theory, *Appl. Optics*, 38, 2346–2357, 1999.
- Myhre, G.: Consistency between satellite-derived and modelled estimates of the direct aerosol effect, *Science*, 325, 187–190, doi:10.1126/science.1174461, 2009.
- Newsom, R. K.: *Doppler Lidar (DL) Handbook*, DOE/SC-ARM-TR-101, ARM Climate Research Facility, USA, 2012.
- Nordbo, A., Järvi, L., and Vesala, T.: Revised eddy covariance flux methodologies - effect on urban energy balance, *Tellus B*, 64, 18184, doi:10.3402/tellusb.v64i0.18184, 2012.
- O'Connor, E. J., Illingworth, A. J., and Hogan, R. J.: A technique for autocalibration of cloud lidar, *J. Atmos. Ocean. Tech.*, 21, 777–786, 2004.
- O'Connor, E. J., Hogan, R. J., and Illingworth, A. J.: Retrieving Stratocumulus Drizzle Parameters Using Doppler Radar and Lidar, *J. Appl. Meteorol.*, 44, 14–27, 2005.
- O'Connor, E. J., Illingworth, A. J., Brooks, I. M., Westbrook, C. D., Hogan, R. J., Davies, F., and Brooks, B. J.: A Method for Estimating the Turbulent Kinetic Energy Dissipation Rate from a Vertically Pointing Doppler Lidar, and Independent Evaluation from Balloon-Borne In Situ Measurements, *J. Atmos. Ocean. Tech.*, 27, 1652–1664, 2010.
- Pappalardo, G., Mona, L., D'Amico, G., Wandinger, U., Adam, M., Amodeo, A., Ansmann, A., Apituley, A., Alados Arboledas, L., Balis, D., Boselli, A., Bravo-Aranda, J. A., Chaikovskiy, A., Comerón, A., Cuesta, J., De Tomasi, F., Freudenthaler, V., Gausa, M., Giannakaki, E., Giehl, H., Giunta, A., Grigorov, I., Groß, S., Haeffelin, M., Hiebsch, A., Iarlori, M., Lange, D., Linné, H., Madonna, F., Mattis, I., Mamouri, R.-E., McAuliffe, M. A. P., Mitev, V., Molero, F., Navas-Guzman, F., Nicolae, D., Papayannis, A., Perrone, M. R., Pietras, C., Pietruczuk, A., Pisani, G., Preißler, J., Pujadas, M., Rizi, V., Ruth, A. A., Schmidt, J., Schnell, F., Seifert, P., Serikov, I., Sicard, M., Simeonov, V., Spinelli, N., Stebel, K., Tesche, M., Trickl, T., Wang, X., Wagner, F., Wiegner, M., and Wilson, K. M.: Four-dimensional distribution of the 2010 Eyjafjallajökull volcanic cloud over Europe observed by EARLINET, *Atmos. Chem. Phys.*, 13, 4429–4450, doi:10.5194/acp-13-4429-2013, 2013.
- Pearson, G., Davies, F., and Collier, C.: An Analysis of the Performance of the UFAM Pulsed Doppler Lidar for Observing the Boundary Layer, *J. Atmos. Ocean. Tech.*, 26, 240–250, 2009.
- Petäjä, T., Laakso, L., Grönholm, T., Launiainen, S., Evelev-Peltoniemi, I., Virkkula, A., Leskinen, A., Backman, J., Manninen, H. E., Sipilä, M., Haapanala, S., Hämeri, K., Vanhala, E., Tuomi, T., Paatero, J., Aurela, M., Hakola, H., Makkonen, U., Hellén, H., Hillamo, R., Vira, J., Prank, M., Sofiev, M., Siitari-Kauppi, M., Laaksonen, A., Lehtinen, K. E. J., Kulmala, M., Viisanen, Y., and Kerminen, V.-M.: In-situ observations of Eyjafjallajökull ash particles by hot-air balloon, *Atmos. Environ.*, 48, 104–112, 2012.
- Portin, H. J., Komppula, M., Leskinen, A. P., Romakkaniemi, S., Laaksonen, A., and Lehtinen, K. E. J.: Observations of aerosol-cloud interactions at the Puijo semi-urban measurement station, *Boreal Environ. Res.*, 14, 641–653, 2009.
- Remer, L. A., Kaufman, Y. J., Tanré, D., Mattoo, S., Chu, D. A., Martins, J. V., Li, R.-R., Ichoku, C., Levy, R. C., Kleidman, R. G., Eck, T. F., Vermote, E., and Holben, B. N.: The MODIS Aerosol Algorithm, Products, and Validation, *J. Atmos. Sci.*, 62, 947–973, 2005.
- Revuelta, M. A., Sastre, M., Fernández, A. J., Martín, L., García, R., Gómez-Morena, F. J., Artñano, B., Pujadas, M., and Molero, F.: Characterization of the Eyjafjallajökull volcano plume over the Iberian Peninsula by lidar remote sensing and ground-level data collection, *Atmos. Environ.*, 48, 46–55, 2012.
- Rolf, C., Krämer, M., Schiller, C., Hildebrandt, M., and Riese, M.: Lidar observation and model simulation of a volcanic-ash-induced cirrus cloud during the Eyjafjallajökull eruption, *Atmos. Chem. Phys.*, 12, 10281–10294, doi:10.5194/acp-12-10281-2012, 2012.
- Rose, T. and Czekala, H.: RPG-XCH-DP X frequency, dual polarized radiometer (6.925/10.65/18.70 (21.00)/36.50GHz h/v), Operating manual, Version 6.8, Radiometer 5 Physics GmbH, Germany, 18 February 2009.
- Rye, B. J. and Hardesty, R. M.: Discrete spectral peak estimation in incoherent back-scatter heterodyne lidar. I: Spectral accumulation and the Cramer-Rao lower bound, *IEEE T. Geosci. Remote*, 31, 16–27, 1993.
- Saltikoff, E., Tuovinen, J.-P., Kotro, J., Kuitunen, T., and Hohti, H.: A climatological comparison of radar and ground observations of hails in Finland, *J. Appl. Meteorol. Clim.*, 49, 101–114, 2010.
- Saltikoff, E. and Neuvonen, L.: First experiences of the operational use of a dual-polarisation weather radar in Finland, *Meteorol. Z.*, 20, 323–333, 2011.
- Schobesberger, S., Väänänen, R., Leino, K., Virkkula, A., Backman, J., Pohja, J., Siivola, E., Franchin, A., Mikkilä, J., Paramonov, M., Aalto, P. P., Krejci, R., Petäjä, T., and Kulmala, M.: Airborne measurements over the boreal forest of southern Finland during new particle formation events in 2009 and 2010, *Boreal Environ. Res.*, 18, 145–163, 2013.
- Shupe, M. D., Turner, D., Walden, V. P., Bennartz, R., Cadetdu, M. P., Castellani, B. B., Cox, C. J., Hudak, D. R., Kulie, M. S., Miller, N. B., Neely III, R. R., Neff, W. D., and Rowe, P. M.: High and dry, new observations of tropospheric and cloud properties above the Greenland ice sheet, *B. Am. Meteorol. Soc.*, 94, 169–186, 2013.
- Sicard, M., Guerrero-Rascado, J. L., Navas-Guzmán, F., Preißler, J., Molero, F., Tomás, S., Bravo-Aranda, J. A., Comerón, A., Rocadenbosch, F., Wagner, F., Pujadas, M., and Alados-Arboledas, L.: Monitoring of the Eyjafjallajökull volcanic aerosol plume over the Iberian Peninsula by means of four EARLINET lidar stations, *Atmos. Chem. Phys.*, 12, 3115–3130, doi:10.5194/acp-12-3115-2012, 2012.
- Souch, C. and Grimmond, S.: Applied climatology: urban climate, *Progress Phys. Geography*, 30, 270–279, 2006.
- Sundström, A.-M., Nousiainen, T., and Petäjä, T.: On the quantitative low-level aerosol measurements using a ceilometer-type lidar, *Atmos. Ocean. Technol.*, 26, 2340–2352, doi:10.1175/2009JTECHA1252.1, 2009.

- Tonttila, J., O'Connor, E. J., Niemelä, S., Räisänen, P., and Järvinen, H.: Cloud base vertical velocity statistics: a comparison between an atmospheric mesoscale model and remote sensing observations, *Atmos. Chem. Phys.*, 11, 9207–9218, doi:10.5194/acp-11-9207-2011, 2011.
- Twomey, S.: Pollution and the planetary albedo, *Atmos. Environ.*, 8, 1251–1256, 1974.
- Vaisala: Ceilometer CT25K User's Guide, Vaisala, available at: <http://www.rish.kyoto-u.ac.jp/ear/ceilometer/ct25k.pdf>, last access: 26 February 1999.
- van Ulden, A. P. and Wieringa, J.: Atmospheric boundary layer research at Cabauw, *Bound.-Lay. Meteorol.*, 78, 39–69, 1996.
- Vesala, T., Haataja, J., Aalto, P., Altimir, N., Buzorius, G., Garam, E., Hämeri, K., Ilvesniemi, H., Jokinen, V., Keronen, P., Lahti, T., Markkanen, T., Mäkelä, J. M., Nikinmaa, E., Palmroth, S., Palva, L., Pohja, T., Pumpanen, J., Rannik, U., Siivola, E., Ylitalo, H., Hari, P., and Kulmala, M.: Long-term field measurements of atmosphere-surface interactions in boreal forest combining forest ecology, micrometeorology, aerosol physics and atmospheric chemistry, *Trends in Heat, Mass Momentum Trans.*, 4, 17–35, 1998.
- Verheggen, B., Cozic, J., Weingartner, E., Bower, K., Mertes, S., Connolly, P., Gallagher, M., Flynn, M., Choulaton, T., and Baltensberger, U.: Aerosol partitioning between the interstitial and the condensed phase in mixed-phase clouds, *J. Geophys. Res.*, 112, D23202, doi:10.1029/2007JD008714, 2007.
- Wandinger, U. and Ansmann, A.: Experimental determination of the lidar overlap profile with Raman lidar, *Appl. Optics*, 41, 511–514, 2002.
- Weitkamp, C.: Lidar: range-resolved optical remote sensing of the atmosphere, in: *Springer series of Optical Sciences*, vol. 102, Springer, 460 pp., 2005.
- Westbrook, C. D., Illingworth, A. J., O'Connor, E. J., and Hogan, R. J.: Doppler lidar measurements of oriented planar ice crystals falling from supercooled and glaciated layer clouds, *Q. J. Roy. Meteorol. Soc.*, 136, 260–276, 2010a.
- Westbrook, C. D., Hogan, R. J., O'Connor, E. J., and Illingworth, A. J.: Estimating drizzle drop size and precipitation rate using two-colour lidar measurements, *Atmos. Meas. Tech.*, 3, 671–681, doi:10.5194/amt-3-671-2010, 2010b.
- Williams, J., Crowley, J., Fischer, H., Harder, H., Martinez, M., Petäjä, T., Rinne, J., Bäck, J., Boy, M., Dal Maso, M., Hakala, J., Kajos, M., Keronen, P., Rantala, P., Aalto, J., Aaltonen, H., Paatero, J., Vesala, T., Hakola, H., Levula, J., Pohja, T., Herrmann, F., Auld, J., Mesarchaki, E., Song, W., Yassaa, N., Nölscher, A., Johnson, A. M., Custer, T., Sinha, V., Thieser, J., Pouvesle, N., Taraborrelli, D., Tang, M. J., Bozem, H., Hosaynali-Beygi, Z., Axinte, R., Oswald, R., Novelli, A., Kubistin, D., Hens, K., Javed, U., Trawny, K., Breitenberger, C., Hidalgo, P. J., Ebben, C. J., Geiger, F. M., Corrigan, A. L., Russell, L. M., Ouwersloot, H. G., Vilà-Guerau de Arellano, J., Ganzeveld, L., Vogel, A., Beck, M., Bayerle, A., Kampf, C. J., Bertelmann, M., Köllner, F., Hoffmann, T., Valverde, J., González, D., Riekkola, M.-L., Kulmala, M., and Lelieveld, J.: The summertime Boreal forest field measurement intensive (HUMPPA-COPEC-2010): an overview of meteorological and chemical influences, *Atmos. Chem. Phys.*, 11, 10599–10618, doi:10.5194/acp-11-10599-2011, 2011.
- Wood, C. R.: Adapting our cities for future climates, *Weather*, 65, 307–309, 2010.
- Wood, C. R., Arnold, S. J., Balogun, A. A., Barlow, J. F., Belche, S. E., Britter, R. E., Cheng, H., Dobre, A., Lingard, J. J. N., Martin, D., Neophytou, M., Petersson, F. K., Robins, A. G., Shallcross, D. E., Smalley, R. J., Tate, J. E., Tomlin, A. S., and White, I. R.: Dispersion experiments in central London: the 2007 DAPPLE project, *B. Am. Meteorol. Soc.*, 90, 955–969, 2009a.
- Wood, C. R., O'Connor, E. J., Hurley, R., Reynolds, D. R., and Illingworth, A. J.: Cloud-radar observations of insects in the UK convective boundary layer, *Meteorol. Appl.*, 16, 491–500, 2009b.
- Wood, C. R., Pauscher, L., Ward, H. C., Kotthaus, S., Barlow, J. F., Gouvea, M., Lane, S. E., and Grimmond, C. S. B.: Wind observations above an urban river using a new lidar technique, scintillometry and anemometry, *Sci. Total Environ.*, 442, 527–533, 2013a.
- Wood, C., Järvi, L., Kouznetsov, R., Nordbo, A., Drebs, A., Vihma, T., Hirsikko, A., Suomi, I., Fortelius, C., O'Connor, E., Haapanala, S., Moilanen, J., Kangas, M., Karppinen, A., Joffre, S., Vesala, T., and Kukkonen, J.: An overview on the Urban Boundary-layer Atmosphere Network in Helsinki, *B. Am. Meteorol. Soc.*, 94, 1675–1690, doi:10.1175/BAMS-D-12-00146.1, 2013b.